Check for updates

Recent advances on nanomaterial-based glutathione sensors

Saman Bagherpour [ID] [ab] and Lluïsa Pérez-García [ID] *[ab]

Glutathione (GSH) is one of the most common thiol-containing molecules discovered in biological systems, and it plays an important role in many cellular functions, where changes in physiological glutathione levels contribute to the progress of a variety of diseases. Molecular imaging employing fluorescent probes is thought to be a sensitive technique for online fluorescence detection of GSH. Although various molecular probes for (intracellular) GSH sensing have been reported, some aspects remain unanswered, such as quantitative intracellular analysis, dynamic monitoring, and compatibility with biological environment. Some of these drawbacks can be overcome by sensors based on nanostructured materials, that have attracted considerable attention owing to their exceptional properties, including a large surface area, heightened electro-catalytic activity, and robust mechanical resilience, for which they have become integral components in the development of highly sensitive chemo- and biosensors. Additionally, engineered nanomaterials have demonstrated significant promise in enhancing the precision of disease diagnosis and refining treatment specificity. The aim of this review is to investigate recent advancements in fabricated nanomaterials tailored for detecting GSH. Specifically, it examines various material categories, encompassing carbon, polymeric, quantum dots (QDs), covalent organic frameworks (COFs), metal–organic frameworks (MOFs), metal-based, and silicon-based nanomaterials, applied in the fabrication of chemo- and biosensors. The fabrication of nano-biosensors, mechanisms, and methodologies employed for GSH detection utilizing these fabricated nanomaterials will also be elucidated. Remarkably, there is a noticeable absence of existing reviews specifically dedicated to the nanomaterials for GSH detection since they are not comprehensive in the case of nano-fabrication, mechanisms and methodologies of detection, as well as applications in various biological environments. This research gap presents an opportune moment to thoroughly assess the potential of nanomaterial-based approaches in advancing GSH detection methodologies.

1. Introduction

Glutathione (GSH) is among the prevalent thiol-containing compounds found in biological systems, contributing significantly to numerous cellular functions.[1] Particularly, biothiols serve as defenders, safeguarding cellular constituents against damage resulting from and reactive oxygen species (ROS) and free radicals.[2] GSH serves as a vital cofactor in numerous biological processes, including catabolism, drug transportation, and detoxification.[3] It plays a role in facilitating cell communication *via* gap junctions and generally protects protein-SH groups from oxidation and crosslinking.[4] Additionally, GSH is crucial for maintaining ascorbic acid in its reduced state and for the formation of deoxyribo-nucleotides.[5]

GSH (Fig. 1) stands out as a tripeptide composed of three amino acids (glutamine, cysteine, and glycine) present within living cells, with concentrations typically falling between 0.5 to 10 mM. In physiological fluids, it is detected at levels approximately ranging from 2 to 12 μM in healthy individuals.[6] Alterations in physiological GSH levels contribute to the onset of various diseases, including Parkinson's,[7] Alzheimer's,[8] diabetes mellitus,[9] and aging-related ailments.[10,11] Additionally, such changes are implicated in various forms of cancer, including breast cancer[12,13] and colorectal cancer.[14,15] Thus, the information provided above clearly highlights the significance of detecting and quantifying GSH in biological and pharmaceutical matrices, whether as a biomarker or as a supplementary drug.

Molecular imaging with fluorescent probes is expected to be a sensitive method for real-time detection of GSH. This strategy has been thoroughly explored and reviewed at the molecular

*[a] Departament de Farmacologia, Toxicologia i Química Terapèutica, Universitat de Barcelona, Av. Joan XXIII 27-31, Barcelona, 08028, Spain.
E-mail: mlperez@ub.edu*
[b] Institut de Nanociència i Nanotecnologia IN2UB, Universitat de Barcelona, Barcelona, 08028, Spain

This journal is © The Royal Society of Chemistry 2024

J. Mater. Chem. B, 2024, **12**, 8285–8309 | **8285**

level,[25–30] using a variety of chemo-sensors and analytical techniques. Although these probes have made great progress, there are still a number of challenges, such as the capacity for conducting quantitative analysis within cells, facilitating real-time monitoring of GSH concentrations, and guaranteeing suitability for complex environments, that need to be overcome. Nonetheless, the relationship between of GSH sensing and nanomaterials has yet to be thoroughly evaluated, highlighting a crucial need in current research efforts. Exploring this intersection could lead to developing innovative and more efficient GSH detection methods especially in the biological environment.

Furthermore, over the past two decades, nanostructured materials have attracted substantial attention due to their exceptional features, and they have been consistently employed as efficient materials in the creation of highly sensitive chemo-sensors[31,32] and biosensors,[33,34] thanks to notable characteristics such as high surface area, improved electrocatalytic activity, and physical resilience.[35] Moreover, engineered nanomaterials exhibited considerable potential in enhancing both the accuracy of disease diagnosis[36–38] and the specificity of treatment approaches.[39–41]

The objective of this review is to explore the recent advancements in the fabricated nanomaterials for detecting GSH (Fig. 1). Specifically, it focuses on the utilization of different categories of materials, including carbon, polymeric, quantum dots (QDs), covalent organic frameworks (COFs), metal–organic frameworks (MOFs), metal-based, and silicon-based nanomaterials for the fabrication of chemo- and biosensors (Fig. 1). The mechanism and approaches of GSH detection using the fabricated nanomaterials will be also explained in the detail, and the limit of detection (LOD), selectivity, and the applied matrix related to different nanomaterial-based GSH sensors are compared as shown in Table 1. To the best of our knowledge, there is no existing review specifically focused on the fabrication and application of various types of nanomaterials for GSH detection. This gap in the literature presents an opportunity to comprehensively evaluate the potential of nanomaterial-based approaches in the improvement of GSH detection methods.

2. Carbon-based nanomaterials

Carbon-based nanomaterials are ideal for sensing applications due to their high surface area, excellent electrical conductivity, and chemical stability. Their sp^2 hybridization in graphene and carbon nanotubes provides robust π–π interactions and electron mobility.[82] These materials offer exceptional mechanical strength and flexibility due to their strong carbon–carbon covalent bonds. They can be functionalized with various chemical groups, enhancing their selectivity and sensitivity towards specific analytes.[83] These combined physicochemical and chemical properties make carbon-based nanomaterials highly effective for diverse and robust sensing solutions. Fullerenes,[84] carbon nanotubes (CNTs),[85] graphene (G) and its derivatives graphene oxide (GO),[86] and nanodiamonds (NDs)[87] are all examples of carbon-based nanomaterials. The main potential biological uses of these nanomaterials are photothermal and photodynamic therapy,[88] as well as bioimaging,[89] fluorescent labelling of cells,[90] stem cell engineering,[91,92] biosensing,[93,94] and drug/gene delivery.[95,96] Since some of them have inherent fluorescence, a narrow emission spectrum that can be tuned, and good photostability, it may be used to image and diagnose cells and tissues.[16,97] Moreover, their surfaces can be altered with functional groups (carboxylic acid, hydroxyl, and epoxy) to improve their characteristics.[98] Carbon-based nanomaterials are mostly preferred and one of the alternatives for GSH detection due to their high surface areas, optical, mechanical, and electrical features.

Saman Bagherpour

Saman Bagherpour received his BSc. in Applied Chemistry from Bu-Ali Sina University, Iran, in 2013 and MSc. in Chemical Engineering from the University of Tehran, Iran, in 2017. He is currently a PhD student under the supervision of Prof. Lluïsa Pérez-García at Universitat de Barcelona, Spain. His current research focuses on the design and synthesis of organic fluorescent dyes and their conjugation to nanoparticles and microchips for the detection of intracellular biomolecules.

Lluïsa Pérez-García

Lluïsa Pérez-García received her Pharmacy degree and PhD from the Universitat de Barcelona (UB). After a two year stay at the University of Birmingham (UK), in Fraser Stoddart's group, she moved back to the UB where she became Associate Professor (1997). From 2015 to 2020 she was appointed as Anne McLaren Research fellow and then Associate Professor at the University of Nottingham (UK), before returning to UB where she is a Full Professor in the School Pharmacy. Her current interests are in the field of nanomedicine, including the use of nanoparticles and hydrogels to delivery agents for photodynamic therapy, and the bio-functionalization of microchips to interact with living cells.
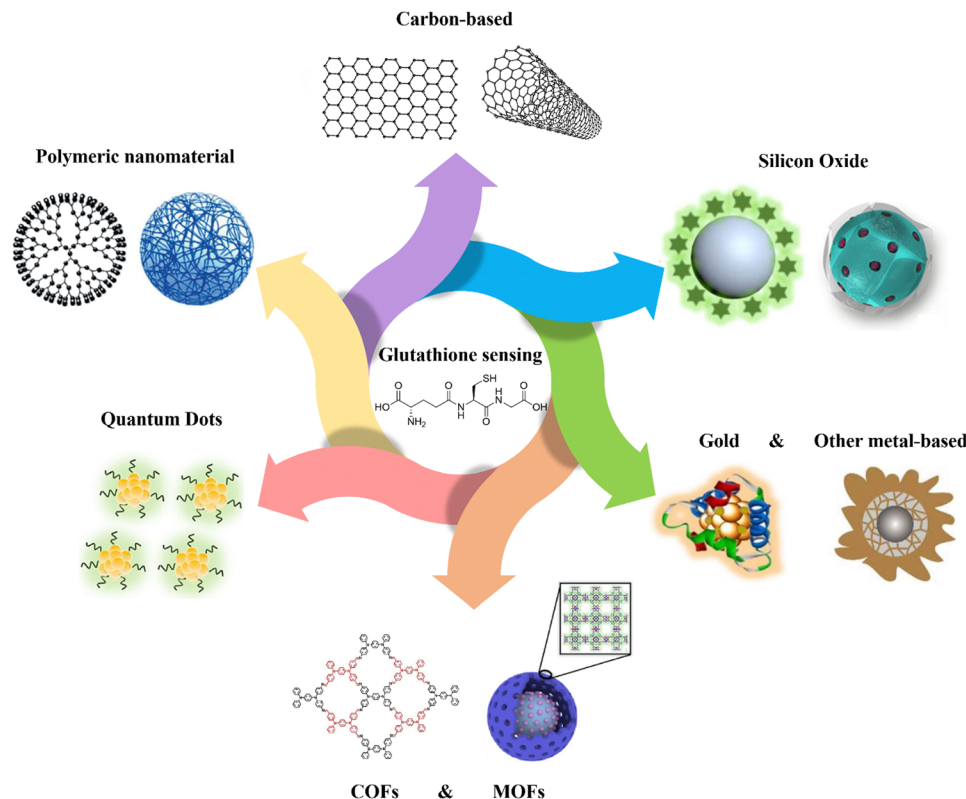
8286 | *J. Mater. Chem. B*, 2024, **12**, 8285–8309

This journal is © The Royal Society of Chemistry 2024

Fig. 1 Schematic representation of various kinds of nanomaterials applied for GSH detection. Carbon-based,[16] polymeric nanomaterial,[17] quantum dots,[18] MOFs,[19] COFs,[20] gold,[21] other metal-based,[22] silicon oxide[23,24] schemes are reproduced with the permission of Elsevier, Springer Nature, American Chemical Society, and Royal Society of Chemistry.

A novel chromogenic probe (CP) for thiols was produced[42] employing an independent fluorophore thiols detection, g-C_3N_4 nanosheets, leading to the fabrication of a fluorescent sensor for the detection of GSH. It utilized the inner filter effect (IFE) to operate as a GSH sensor (Fig. 2(a)). In order to produce an efficient IFE system, CP molecules were adsorbed on the g-C_3N_4 nanosheets surface through the contact of π–π- stacking.[99] This sensor has a more evident fluorescence response for GSH with limit of detection of 0.01 μM than Cys, Hcy, and Lys. When CP and GSH react, the nucleophilic addition of GSH destroys the CP's – conjugated structure, resulting in the formation of the non-conjugated product CP–SR. High fluorescence quenching efficiency is achieved when the molar ratio of g-C_3N_4 nanosheets to CP is 1 : 250.

Carbon dot-based photoelectrochemical (PEC) sensors have been also developed for ultrasensitive GSH detection.[43] The best detecting qualities were demonstrated by the nanocomposite of carbon dots mesoporous silica (CDs@MS) based PEC sensors among the various hybrid nanocomposites. In a PEC sensing system, CDs demonstrate both photoelectric and catalytic capabilities. To further improve the catalytic capabilities of CDs and get improved GSH detection efficiencies, graphene oxide (GO), silver nanoparticles (AgNPs), and mesoporous silica (MS) were incorporated as a nanocomposite. The increased photocurrent amplitude observed with rising the levels of GSH at positive potentials demonstrated that the designed PEC catalyses the oxidation of GSH.

An innovative and straightforward approach has been also applied for the fluorescence detection of GSH on the basis of the inhibitory impact of GSH on the magnetic nanoporous graphene (MNPG)-catalysed oxidation of thiamine,[44] which generated fluorescence (Fig. 2(b)). This provides a quick and easy technique for producing porous graphene by partially combusting Hydrotalcite-imperfectly coated graphene oxide. These factors may contribute to MNPG's strong catalytic activity for the following reasons. First, due to the combination of porous structures and good intrinsic properties of graphene, the 3D architectures of NPG might offer high surface area as well as quick mass and electronic transfer kinetics. Second, Fe_3O_4 might prevent the graphene layers aggregation and third, NPG and Fe_3O_4 work synergistically in the nanocomposite. Following the addition of GSH, the fluorescence decreased because the competing oxidations of thiamine[100] and GSH inhibited the oxidation of thiamine.

A new plasmonic detecting system was developed using plasmon hybridization in graphene nanoribbons/silver nanoparticles (GNR/AgNPs) nanocomposites,[45] for the consecutive colourimetric determination of dopamine (DA) and GSH in human blood serum. To explore the plasmonic influence of carbon-based nanostructures on the sensor's capability, the performance of the hybrid GNR/Ag NPs with graphene oxide (GO) and multiwall carbon nanotube (MWCNT) was compared. Hence, colourimetric detection of DA and GSH was carried out employing variations in the location and strength of the

This journal is © The Royal Society of Chemistry 2024

J. Mater. Chem. B, 2024, **12**, 8285–8309 | 8287

Table 1 List of nanomaterial-based GSH sensors and corresponding methodology, limit of detections, interferences, and applied matrix for the of GSH detection. For the interferences of other analytes

Type	Name and role of nanomaterial in sensing	Methodology	Linear range	Limit of detection	Interferences of other analytes	Toxicity	Matrix	Ref.
Carbon-based	g-C$_3$N$_4$ nanosheets/chromogenic probe (inner filter effect)	Fluorescence assay	0.05 μM to 1.0 μM	0.01 μM	Low[a] for (Cys, Hcy, and Lys)	Not mentioned	Human serum	42
	AgNPs/graphene oxide/mesoporous silica (catalytic activity)	Electrochemical	0.02 μM to 4 μM	6.2 nM	Low for (Hcy), (Cys), (Tyr), (Thr), (Val), (Phe), (Asp), (AA), (DA), (Leu), (Glu), (Arg), (Lys), (Trg), (His), (Ser)	Not mentioned	Human serum/myocardial infarction model of mice	43
	Magnetic nanoporous graphene nanocomposites (catalytic activity)	Fluorescence Assay (oxidation of thiamine)	0.2 μM to 20 μM	0.05 μM	Low for (Cys), (Lys), (Arg), (AA), (His), (Met), (Tyr), (Trp), (Phe), (Hcy), (Ile), (Thr), (Ala), (Ser), (Val), (Gly)	Not mentioned	PC12 Cell Lysate	44
	Graphene nanoribbons/silver nanoparticles (plasmonic absorption band of AgNPs)	Fluorescence assay/colourimetric	1 μM to 75 μM	0.23 μM	Low for (AA), (Gluc), (Glu), (Cys), (Trp), (Phe), oxalic acid, urea, citric acid, K$^+$, Na$^+$, Ca^{2+}, Cu^{2+} and Mg^{2+})	Not mentioned	Human serum	45
	Iron phthalocyanine, N, B-doped reduced GO (catalytic activity)	Electrochemical	5.0×10^{-8} M to 1.6×10^{-3} M	7.1×10^{-9} M	Low for (Hcy, Glu, Tyr, Cys, Arg, Trp, Lys, DA, UA, AA)	Not mentioned	Human serum	46
	N,S co-doped carbon quantum dots (fluorescence alteration)	Fluorescence assay	0 to 100 μM	6.7 μM	Low for (His, Trp, Thr, Arg, Ser, Asp, Val, Leu, Gly, Lys, Cys, and Hcy)	Low cytotoxicity	HaCaT cells	47
	N-doped carbon dots/TNB(inner filter effect)	Fluorescence Assay/colourimetric	0.2 μM to 1000 μM	30 nM	High[b] for (Hcy and Cys), Low for (Pro, Arg, Nleu, Orn, Tyr, Asp, Phe, Ser, His, Trp, Thr, Val, Glu, Ileu, Gly, Lys, Asn, Ala)	Low cytotoxicity	SMMC-7721 cells	48
	Graphitic carbon nitride (g-C$_3$N$_4$)-Cu^{2+} (photoinduced electron transfer)	Fluorescence Assay	0.05 μM to 900 μM	20 nM	Low for (AA, Ala, His, Ser, GS, Try, Glu, Arg, Ala, Lys, Cys)	Not mentioned	Tomato extract	49
Polymeric-based	Green-fluorescent polydopamine nanoparticles (fluorescence quenching)	Fluorescence assay	2.20×10^{-5} M to 2.49×10^{-6} M	2.84×10^{-7} M	Low (AA, Ala, His, Ser, GS, Try, Arg, Glu, Lys, Ala, Cys, Hcy, Meth)	Not mentioned	Urine and Saliva	50
	Polymer dots (PDs) can be suppressed by MnO$_2$ nanosheets (fluorescence quenching)	Fluorescence Assay	0.5 μM to 200 μM	0.10 μM	Low (AA, Cys, Hcy, Glu, His, Gly, Gln, Lys, Ala, and Tyr)	Not mentioned	Human serum	51
	Hemin-encapsulated recombinant camel serum albumin nanocomposite (peroxidase mimic activity)	Absorption assay/colourimetric	3.2 μM to 100 μM	0.667 μM	Low (Cys, Trp, His, BSA, Ala)	Not mentioned	Fetal bovine and human serum	52
	Exopolysaccharide/MnO$_2$/fluorescein(fluorescence alteration)	Fluorescence assay	0.05 mM to 4 mM	0.16 μM	High for Cys. Low for (Hcy, Val, Met, Gly)	Low cytotoxicity	HPAEpiC cells just for biocompatibility	53
	ADA-Au-FF-dye nanospheres (fluorescence quenching)	Fluorescence Assay	0 μM to 200 μM and 1 μM to 15 mM	—	High (Cys). Low for other type amino acids	Low cytotoxicity	293T cells and HeLa cells	54
	Fluorescent polydopamine nanoparticles/CoOOH (oxidation of GSH)	Fluorescence assay	10 μM to 500 μM	3.25 μM	High interference of Cys (Cysteine), homocysteine (Hcy) and vitamin C	Not mentioned	Human serum	55
	N-doped carbonized polydopamine nanotubes (peroxidase-like activity)	Electrochemical/Absorption Assay (oxidation of TMB)	0.6 μM to 60 μM	0.2 μM	Not mentioned	Not mentioned	Human serum	56
	DQ-CD@Pdots (fluorescence alteration)	Fluorescence Assay	0.01 μM to 3 μM	2.7 nM	High interference of Cys and AA. Low interference of other amino acids	Low cytotoxicity	HeLa cells and zebrafish	57
MOFs & COFs	Ce-MOF/AuNPs (fluorescence alteration because of FRET)	Fluorescence assay	0.2 μM to 32.5 μM	58 nM	Low (AA, His, Iso, Ala, Ser, Leu, Lys, Met, Thr, DL-Pro Val, Try, DL-Cys, Glu-A, Gly, Cys, Tyr)	Not mentioned	Human serum	58
	[Co(L)(H$_2$O)$_2$] MOF (peroxidase-like activity)	Chemiluminescence assay	0.05 μM to 2.0 μM	0.03 μM	High interference of AA. Low interference (L-Cys and other amino acids)	Not mentioned	Human breast cancer and laryngeal cancer cells lysates	59
	Au@Cu-MOF nanocapsules (electrocatalytic activity for GSH detection)	Electrochemical	0.01 nM to 40 nM and 40 nM to 10 μM	2.5 pM	Low interference Cys, Hcy, and other amino acids	Not mentioned	Human serum, tomato, cucumber	39

8288 | J. Mater. Chem. B, 2024, 12, 8285–8309

This journal is © The Royal Society of Chemistry 2024

Table 1 (continued)

Type	Name and role of nanomaterial in sensing	Methodology	Linear range	Limit of detection	Interferences of other analytes	Toxicity	Matrix	Ref.
	Donor-acceptor Py–TT COFs (enzyme-like catalytic capabilities)	Absorption Assay (oxidation of TMB)	0.4 μM to 60 μM	0.225 μM	Not mentioned	Not mentioned	Human serum	60
	TTAP-COF nanosheet (catalytic activity)	Absorption Assay (oxidation of TMB)	0.5 μM to 40 μM	0.5 μM	Low interference Ala, Arg, Glu, Asp, Ile, Ser, Tyr, Thr, Cys, AA.	Not mentioned	Standard GSH solution	20
	COF-300-AR (enzyme-mimicking activity)	Absorption assay (oxidation of TMB)	1 μM to 15 μM	1.0 μM	High interference L-Cys, AA, Hcy, and SO_3^{2-}. Low ((Arg), (Thr), (Leu) (Glu), (Gly))	Not mentioned	HL60 cell lysate	61
	COFs-MnO₂ (fluorescence alteration)	Fluorescence assay	0.5 μM to 100 μM	0.28 μM	Low interference (metal ions (Na^+, K^+, Ca^{2+}, Mg^{2+} and Mn^{2+}), protein (BSA), carbohydrate (Suc, Man, Fru, Glu and Gal), amino acids (Phe, Lys, Nva, Gly, Ile, Arg, His, Met, Thr, Leu, Hcy and Cys), urea and AA)	Not mentioned	Human serum	62
	FeS₂@SNW-1 (peroxidase-like nanozyme)	Electrochemical/ Fluorescence Assay/ Test strips	Fluorescence (4.46 μM to 1.14 mM)/ Electrochemical (10.69–452.2 μM)	fluorescence (1.61 μM)- Electrochemical (6.23 μM)	Low (Ca^{2+}, NH_4^+, K^+, Zn^{2+}, Mg^{2+}, HPO_4^-, Arg, Gly, Thr, Glu, Leu). Moderate^c (AA, Hcy, Cys)	Not mentioned	H1299 cell lysate	63
Quantum dots (QDs)	Molybdenum disulfide QDs/ MnO₂ nanosheets (fluorescence reduction)	Fluorescence assay/ colourimetric	5.0 μM to 300.0 μM for fluorescence method; 2.0 μM to 300.0 μM for colourimetric method	1.57 μM for fluorescence method, and 0.50 μM for colourimetric method	High (ascorbic acid and cysteine)- Moderate (serine, lysine, glycine, tryptophan), (glucose and BSA)	Not mentioned	Human serum	64
	N-Ti3C2 QDs (fluorescence reporter)	Fluorescence assay/ colourimetric	0.5 μM to 100μM	0.17 μM	Low (L-Gln, L-Cys, D-Asp, Gly, L-Glu, and His)	Low cytotoxicity	MCF-7 cells	65
	VOx QDs-MnO₂ nanosheets (fluorescence alteration)	Fluorescence assay	0.5 μM to 100 μM	0.254 μM	High interference Cys. Low interferences (Cd^{2+}, Na^+, Cu^{2+}, Ca^{2+}, K^+, Ba^{2+}, Co^{2+}, Mg^{2+}, Fe^{3+}, Al^{3+}, Zn^{2+}, Hg^{2+}, Mn^{2+}), anions (NO_3^-, Cl^-, SO_4^{2-}, CO_3^{2-}, Ac^-), amino acids (Phe, Arg, Ser, Ile, Lys, Leu, Val, Pro, Asp, Gly, Met, Glu, L-Glu, Thr, His), and molecules (BSA, urea, AA, glucose)	Not mentioned	Human serum, vegetable, fruit	66
	Orange-emissive sulphur-doped organosilica nanodots (S-OSiNDs) (fluorescence alteration)	Fluorescence assay	0 μM to 100 μM	0.2 μM	Low (Na^+, Ca^{2+}, Mg^{2+}, K^+, L-Glu, L-Lys, Gly, L-Ser, L-Hcy, DL-DTT, ascorbic acid, glucose, L-Cys, DL-Cys, and BSA)	Low cytotoxicity	HPAEpiC and L02 cells	67
	H-SQDs@MnO₂ (ECL response)	Fluorescence assay	0.05 μM to 5.0 μM	35 nM	Low (metal ions (Mg^{2+}, K^+, Na^+, Fe^{3+}, Ca^{2+}, Cu^{2+}, Fe^{2+}, Zn^{2+} and Mn^{2+}), amino acids (Lys, Gly, Tyr, Glu, and Cys), saccharide (sucrose and glucose), CA and AA.)	Not mentioned	Human serum	18
	WS2 QDs-MnO₂ (ratio-sensing platform)	Fluorescence assay	0 to 60 μM	0.12 μM	High AA, Low (metal ions (Mg^{2+}, Na^+, K^+, Ca^{2+}, Fe^{3+}, and Zn^{2+}), amino acids (Tyr, Hcy, Gly, Cys, Ser, and His), and biomolecules (galactose, BSA, and glucose)	Not mentioned	Human serum, lake water and tap water	68
	CdTe QD-polynitroxylated albumin (fluorescence alteration)	Fluorescence assay	5 μM to 60 μM	20 nM	Moderate (Cys or Hcy)	Low cytotoxicity	MCF-7 (cancer) and Hs578Bst (normal) cells	69
Gold and other metals	BPQDs@MnO₂ (fluorescence quenching)	Fluorescence assay	0.1 μM to 60 μM	35 nM	High Cys. Low for other amino acids, glucose and metal ions	Low cytotoxicity	A549 cells	70
	AuNPs (aggregation and anti-aggregation of AuNPs in the presence GSH)	Absorption assay	0.1 μM to 1.0 μM.	12.0 nM	Moderate (GSSG). Low (amino acids (Tyr, His, Lys, Ala, Val, Asn, Arg, Trp, Met, Asp, Gln, Glu, Gly, Ile, Leu, Phe, Thr, Pro, Ser), two analogous biothiols (Hcy and Cys), anions ($H_2PO_4^-$) cations (K^+, Mg^{2+}, Ca^{2+}, Na^+, and NH_4^+)	Not mentioned	Human urine and human serum	71

This journal is © The Royal Society of Chemistry 2024

J. Mater. Chem. B, 2024, 12, 8285–8309 | 8289

Table 1 (continued)

Type	Name and role of nanomaterial in sensing	Methodology	Linear range	Limit of detection	Interferences of other analytes	Toxicity	Matrix	Ref.
	Gold-silver bimetallic nanocluster (fluorescence alteration)	Fluorescence Assay	1 µM to 100 µM	200 nM	Moderate (Cys, Met and AA). Low (sucrose, glucose, GSSG, AA, DA, and cations including Zn^{2+}, K^+, Na^+ and Ca^{2+})	Not mentioned	Human serum	21
	Gold-viral biomineralized nanoclusters (AuVCs) (catalytic activity)	Colourimetric GSH detection using AuVCs through TMB/H_2O_2	25 µM to 500 µM	9.8 µM	Moderate (Cysteine, cystamine), Low (PRO-PREP™ cell lysing buffer, IgG, DNA, cell extracted total RNAs and BSA).	Not mentioned	cell lysate protein	72
	Gold nanocrystals (peroxidase-like activity)	Colourimetric, Absorption Assay (oxidation of TMB)	2 µM to 25 µM	420 nM	High (Cys, and Hcy). Low (Met, Phe, Ser, Lys, Ala, Thr, Asp, Gly, Glu, Gln, Arg, Tyr, Pro, Try, Val, Ile, and His)	Not mentioned	Cancer cells (MDA-MB-231 and MCF-7) and Normal cells (HBE and THP-1) lysates	73
	AuNCs-Carbon dots-Cu (fluorescence alteration)	Fluorescence assay/paper strip	0 µM to 50 µM for Fluorescence Assay/ 0–50 µM paper strip	0.76 µM for Fluorescence Assay/ 1.84 µM for paper strip	High (Cys and Hcy). Low (metal ions (Ca^{2+}, Na^+, Fe^{2+}, K^+) glucose, sucrose, Glu, Gly, Arg, Leu, Val, Ala, Thr, BSA, AA, CSSG)	Not mentioned	Human serum	74
	Fe-doped MoS$_2$ (catalytic activity)	Colourimetric, absorption assay (oxidation of TMB)	1 µM to 30 µM	0.577 µM	Moderate (Cys, Hcy). Low (Glu, Tyr, Pro, Gly, Met, His, Asp, Lys, Ala, Leu)	Not mentioned	Human serum	75
	MXene@NiFe-LDH (catalytic activity)	Colourimetric, absorption assay (oxidation of TMB)	0.9 µM to 30 µM	84 nM	Low (isoleucine, arginine, histidine, tryptophan, leucine, serine), metal ions (Ca^{2+}, Mg^{2+}, Fe^{3+}, K^+, Na^+), urea, glucose, ascorbic acid, and uric acid	Not mentioned	Standard GSH solutions	76
	MnO$_2$-coupled UCNPs (fluorescence alteration)	Colourimetric, absorption assay	0 µM to 350 µM	0.68 µM	Low (Cys, Hcy, Clu, Gly)	Not mentioned	Standard GSH solutions	22
	Mixed-valence-state cobalt (MVSC) (catalytic activity)	Colourimetric	0.5 µM to 40 µM	0.03 µM	High (Cys, Hcy). Low (Val, Lys, Try, Leu, Met, Thr, Phe, and Ile,) saccharides (fructose, galactose, maltose, and glucose), cations (K^+, Mg^{2+}, Na^+, Ca^{2+}, Zn^{2+}, and Fe^{3+})	Not mentioned	Eye drops and Chewable tablets	77
Silicon oxide-based	GQDs-SiNPs/GC (improving electrocatalytic activity)	Electrochemical	0.5 µM to 7 µM	0.5 µM	Low (AA, DA, glucose and urea)	Not mentioned	Human serum	78
	MnO$_2$–SiO$_2$ NPs-TPE3 (aggregation-induced emission (AIE))	Fluorescence assay	0.5 µM to 100 µM	200 nM	Low (Cys, Hcy, glucose)	Not mentioned	Human serum	23
	Functionalized mesoporous silica NPs (MSN)-disulphide-oligo(ethylene glycol)-safranin O as a dye (support for functionalization with a dye)	Fluorescence assay	0.1 µM to 10 µM	0.1 µM	Moderate (Cys, Hcy, HS$^-$ and Me$^-$). Low (Cl–, F$^-$, Br$^-$, I$^-$, OH$^-$, CN$^-$, HPO$_4^-$, Citrate, AcO$^-$, N$_3^-$, NO$_3^-$, SO$_3^{-2}$, S$_2$O$_4^{-2}$ and SO$_4^{-2}$), oxidants (H$_2$O$_2$), amino acids (Tyr, His, Glu, Arg, Asp, Ala, Asn, Gln, Trp, Gly, Thr and Val)	Not mentioned	human serum	79
	(FITC)-doped solid SiO$_2$ nanosphere-MnO$_2$ (support for functionalization with a dye)	Fluorescence assay	10 µM to 300 µM	2.1 µM	High (Cys, Hcy). Moderate (Leu, Met, Lys, Tyr, Ile, Asp, Thr, Ala, Val, Trp, Phe, HSA, Gly, and Glu)	low cytotoxicity	Human blood serum and HeLa cells	80
	Thymine-Hg^{2+}–thymine (T-Hg^{2+}-T)-Mesoporous silica NPs(support for functionalization with a dye)	Electrochemical	1.0 nM to 1.0 µM	0.6 nM	Low (Ser, Phe, Lys, Arg, Trp, Asp, Glu, His, GSSG and GGG)	Not mentioned	Standard GSH solutions	81
	Gated aminated mesoporous silica NPs-MnO$_2$ nanosheet (support for loading nanoparticles)	Portable glucose meter (release of loaded glucose from the pores of MSNs)	100 nM to 10 µM	34 nM	Low (Glu, Gly, Asp, Tyr, Lys, and AA)	Not mentioned	Human serum	24

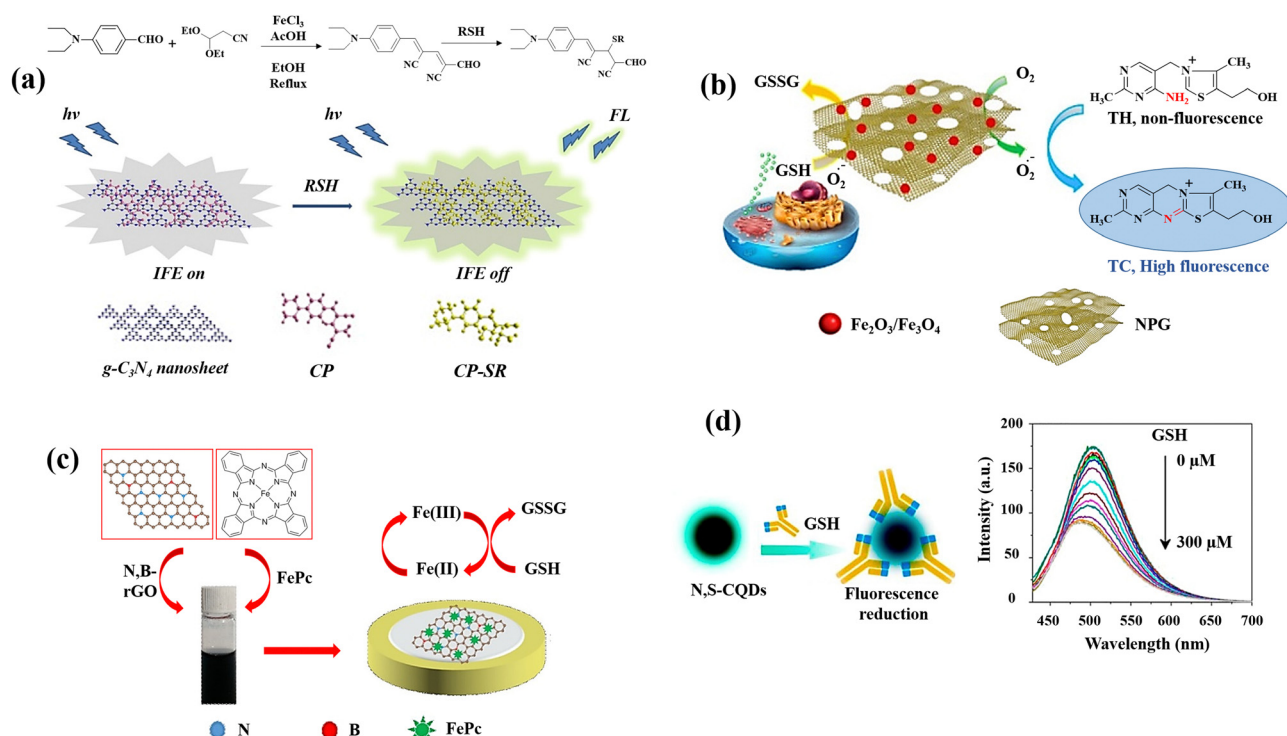^{a} Low: interferences less than 5%. ^{b} High: interferences more than 80%. ^{c} Moderate: interferences more about 20–30%.

Fig. 2 Schematic illustration of GSH detection with carbon-based nanomaterials: (a) the IFE-based fluorescence sensor g-C_3N_4 nanosheets/CP,[42] (b) the MNPG-based fluorescent assay,[44] (c) the FePc/N,B−rGO nanocomposite,[46] and (d) graphical example of the of N,S-CQDs fluorescence response to GSH along with the fluorescence spectra of N,S-CQDs combined with different levels GSH[47] reproduced with the permission of Elsevier and American Chemical Society.

localized surface plasmon resonance (LSPR) absorption band. In the presence of DA, the etching process and morphological transition of AgNPs results in a blue shift in the LSPR spectrum of AgNPs. Based on the aggregation of nanoparticles, which resulted in a reduction in the plasmonic absorption band of AgNPs and a shift in colour from red to grey, GSH was successively identified with the linear range of 1 to 75 μM with limit of detection of 0.23 μM using a GNR/Ag NPs-DA mixture.

A simple fabrication method for iron phthalocyanine (FePc) functionalized N,B-doped reduced graphene oxide nanocomposites (FePc/N,B-rGO) (Fig. 2(c)) was reported as an electrochemical platform for sensitive GSH detection.[46] Through π–π interaction, FePc is conjugated to the surface of N,B-rGO, and the resulting nanocomposite provides a larger specific area for the GSH oxidation and increases the effectiveness of electron transfer. The enhanced active surface area of the FePc/N,B-rGO nanocomposites showed that the active surface area of the FePc/N,B-rGO nanocomposites was effectively raised by the of N,B-rGO and FePc combination. The FePc oxidation and subsequent electron transfer from GSH to the oxidized FePc is the potential mechanism for GSH detection.

L-Cysteine (L-cys) and $NH_3 \cdot H_2O$ were also used[47] to prepare multifunctional nitrogen and sulphur co-doped CQDs (N,S-CQDs) by a one-step hydrothermal process. Due to the N,S-CQDs' exceptional ability to distinguish GSH from other bithiols like Cys and Hcy, it can be utilized as a promising sensor reagent for GSH detection. The amino groups on N,S-CQDs can be ionized as a result of the deprotonation of GSH, to form positively charged N,S-CQDs. Electrostatic interactions can result in complexes between the positively charged N,S-CQDs and the negatively charged GS$^-$ leading to the reduction of fluorescence intensity of N,S-CQDs (Fig. 2(d)).

A one-pot method was also used for fabrication of N-doped carbon dots (N-doped CDs), and the reagent 5,5′-dithiobis-(2-nitrobenzoic acid) (DTNB) was utilized to GSH recognition.[48] IFE substantially simplifies the sensor design by eliminating the necessity for surface modification or linkage between the receptor and the fluorophore. The product of reaction with GSH (5-thio-2-nitrobenzoic acid (TNB)) is able to perform as a potent IFE absorber because of its significant molar extinction coefficient.[101] DTNB does not affect the fluorescence intensity of N-doped CDs by itself, but the reaction product of DTNB with GSH has a subtle but considerable effect on the excitation of N-doped CDs, which causes the fluorescence of N-doped CDs to be quenched. That is due to the fact that the absorption band of TNB and the excitation band of N-doped CDs have a good overlap.

Graphitic carbon nitride (g-C_3N_4) nanosheets were employed as a novel carbon-based nanomaterial with a high fluorescence quantum yield and specific surface area.[49] A selective fluorescent sensor for detecting GSH in food samples was developed using an "on–off–on" strategy. The system of detection was devised by suppressing the g-C_3N_4 nanosheets fluorescence with Cu^{2+} via photoinduced electron transfer (PET), and the

This journal is © The Royal Society of Chemistry 2024

J. Mater. Chem. B, 2024, 12, 8285–8309 | 8291

suppressing fluorescence was recovered by Cu^{2+} coordination to GSH. Cu^{2+} chelation with N of the g-C_3N_4 nanosheets brings them close together. Due to the fact that the potential redox of Cu^{2+}/Cu^+ is between the g-C_3N_4's conduction band (CB) and valence band (VB), photoinduced electron transfer (PET) occurs from the CB to the complexed Cu^{2+}, resulting in quenching fluorescence ("off" state). The GSH addition to the system of g-C_3N_4 nanosheet-Cu^{2+} clearly resulted in g-C_3N_4 recovery.

3. Polymer-based nanomaterials

The analysis of biomarkers, diagnostic imaging, immunoassays, and the diagnosis of cancer are amongst the most crucial applications for polymeric nanoparticles (PNPs) in optical diagnostics.[102] The key aspect in the majority of tests based on nanoparticles is the target biomolecule binding to PNPs, which should produce a quantifiable signal that may be used to identify the target analyte.[103] Enzymes can catalyse the formation of coloured compounds, which can be recognized by an alteration in the colour of a solution, or molecules with the ability of fluorescence signal emission,[104] are the most frequently employed labels for this purpose. Inorganic or organic materials can be used to make polymeric nanomaterials, and a variety of techniques, including dispersion, precipitation, and interfacial polymerizations, can be used to form polymeric nanoparticles from monomers.[17,105] Even organic and inorganic polymeric nanomaterials can function as transducers of signal, converting the analyte presence into a measurable optical response brought on by alterations in the fluorophore's photophysical properties, irrespective of the nanomaterial composition.[106] Some studies have also explored the utilization of PNPs in the context of GSH detection.

For instance, the salicylaldehyde-modified green-fluorescent polydopamine PNPs (PDASA PNPs) were produced, analysed, and used[50] for the detection of GSH (Fig. 3(a)). Among the metal ions tested, Cu(II) formed a non-fluorescent complex in the ground state between both the PDASA PNPs and the quencher Cu(II), leading to the reduction of the fluorescence of PDASA NPs. The calculated constant of Stern–Volmer (KSV) confirmed that the fluorescence quenching was naturally static. The quenched fluorescence was recovered with the GSH addition into Cu(II)–PDASA NPs due to the coordinated Cu(II) displacement, resulting in the GSH levels quantification in the samples saliva and urine.

A sensing system in which the fluorescence of the polymer dots (PDs) can be suppressed by MnO_2 nanosheets has been reported.[51] Common methods for producing PDs materials from small molecules or polymers, such as dehydration, condensation, and carbonization, typically result in bright blue fluorescence under ultraviolet irradiation, but this fluorescence is limited in biological applications due to the interference of auto-fluorescence and potential photo-damage in biological tissues. Using hydroquinone and ethylenediamine as precursors, a simple one-step technique for producing PDs with highly green colour fluorescence was presented. It should be

noted that excessive amounts of ascorbic acid and Cys would affect the GSH assay. This research not only offers a technique for effectively detecting GSH, but it also gives information about how fluorescent sensors made of MnO_2 nanosheets are built.

A unique hemin-loaded nanozyme system was developed utilizing recombinant camel serum albumin (rCSA) to harness the exceptional stability of camel serum albumin.[52] The developed hemin-rCSA nanoparticles provide a number of benefits. The obtained hemin-rCSA nanoparticles could be altered in size. Moreover, in comparison to naked hemin and horseradish peroxidase (HRP), the produced hemin-rCSA nanoparticles displayed enzyme-like activity with a greater affinity to the substrate. It was also possible to quickly detect GSH, resulting from the strong hemin-rCSA NPs peroxidase mimic activity, using colourimetry and a smartphone. As a result, the nanozyme that was synthesized via rCSA has enormous promise for designing biosensing kits. A quick and affordable colourimetric analytical approach for the measurement of GSH was created, wherein the oxidation products of 3,3′,5,5′-tetramethylbenzidine (TMB) were reduced by GSH, leading in the illumination of blue solution and GSH detection with the limit of detection of 0.667 μM.

A new chemiluminescence method has been also developed to identify physiological thiols utilizing a nano-probe that has been isoluminol-labeled.[107] N-Succinimidyl-3-(2-pyridyldithio) propionate (SPDP) was used to change the amino group on the magnetic beads (MBs) surface into the groups of pyridyl disulphide while thiolated signal DNA and isoluminol were tagged on polystyrene microsphere's surface (PSMs) (Fig. 3(b)). The thiolated signal DNA and isoluminol molecules conjugated to the surface of modified PSMs were connected to the SPDP activated MBs surface by disulphide bonds to create a chemiluminescence probe. The disulphide bonds might be easily broken in the presence of GSH. The molecules of isoluminol altered on the PSMs surface released from the chemiluminescence probes were magnetically separated and moved to the dark closet for recognition capability of isoluminol–H_2O_2–HRP by the chemiluminescence assay. Moreover, the measurement of the free thiol compounds amount present in cancer cells using the isoluminol–H_2O_2–HRP CL system was reported, the PSM signal amplification, and the innate disulphide bond cleaving that occurs when GSH is present.

An exopolysaccharide (EPS) was isolated from Lactobacillus plantarum R503, a novel type of natural spherical EPS nanoparticle.[53] The EPS-R503 nanoparticles are constituted of negatively charged heteropolysaccharide made up of mannose, glucose, galactose, and glucuronide with a number of functional groups, such as OH, COOH, and NH_2. $KMnO_4$ and EPS nanoparticles form EPS–MnO_2 nanocomposites, followed by fluorescein (FL) adsorption onto the surface of nanocomposites. FL fluorescence intensity which was considerably reduced in EPS–MnO_2–FL nanocomposites can be restored by GSH due to the reduction of MnO_2 to Mn^{2+} ions. Red blood cells obtained from mouse blood and HPAEpiC cells, which are human normal lung cells, were utilized to investigate the effects of cytotoxicity of the EPS–MnO_2–FL nanosheet. MnO_2–EPS–great FL's

8292 | J. Mater. Chem. B, 2024, 12, 8285–8309

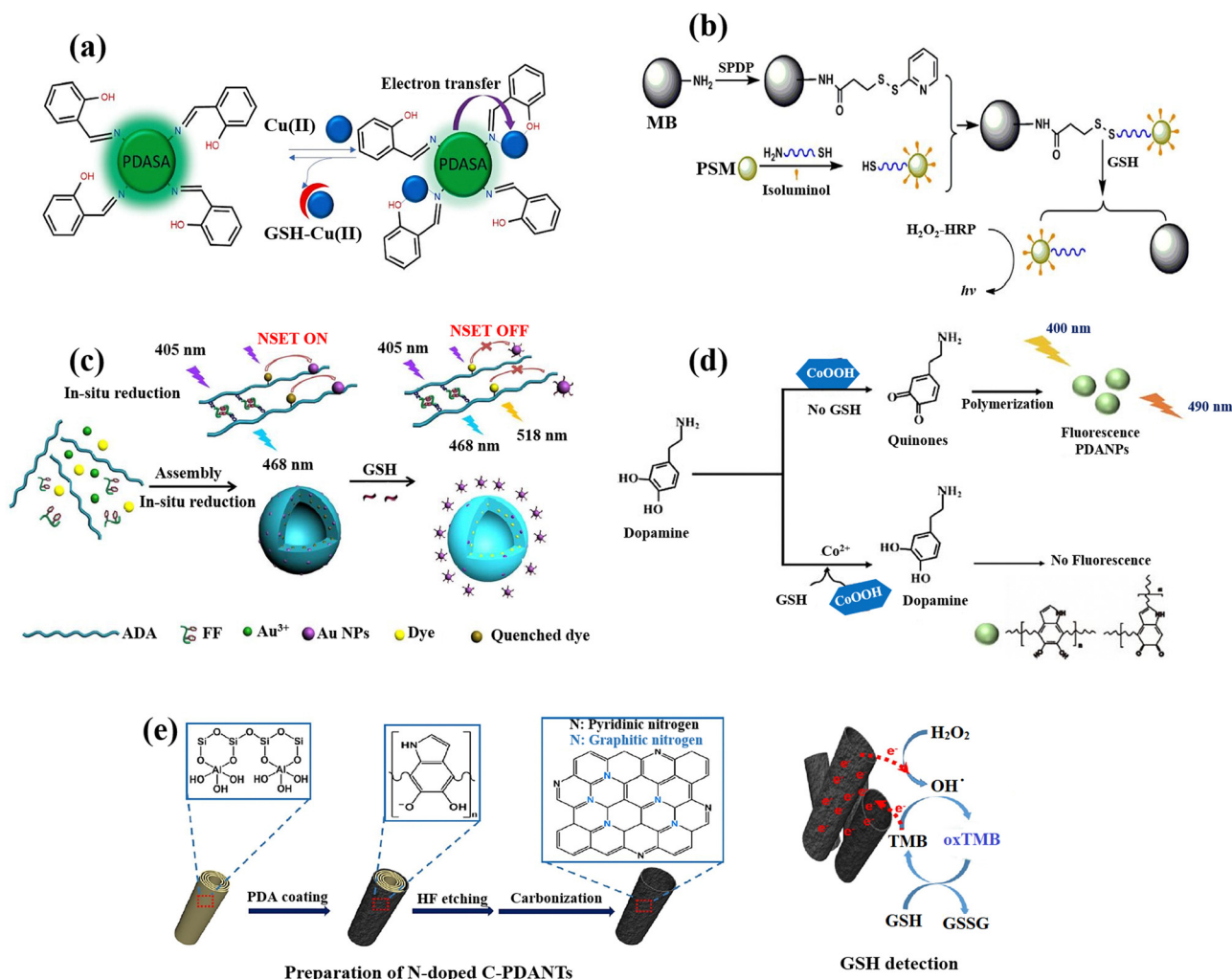This journal is © The Royal Society of Chemistry 2024

Fig. 3 Schematic illustration of GSH detection with polymer-based nanomaterials: (a) Demonstration of fluorescence switching 'on–off–on' of PDASA nanoparticles as Cu(II) and GSH are successively introduced,[50] (b) the scheme of detection process for quantification of the GSH with the bead-isoluminol-PSM probe,[107] (c) preparation of Au-ADA-FF-dye hybrid nanospheres and fluorescent GSH detection strategy,[54] (d) schematic of fluorescent PDA nanoparticles for GSH sensing,[55] (e) the fabrication of N-doped C-PDANTs and GSH recognition based on the N-doped C-PDANTs peroxidase-like activity[56] reproduced with the permission of Elsevier and American Chemical Society.

biocompatibility is advantageous for biomedical applications and allows for *in vivo* measurement of GSH.

The one-pot synthesis of a novel and highly effective ratiometric fluorescent biosensor has been reported[54] by the polysaccharide (alginate dialdehyde, ADA)-dipeptide (diphenylalanine, FF) self-assembly and *in situ* AuNPs reduction while simultaneously the encapsulation of 5-aminofluorescein (FL–NH$_2$) (Fig. 3(c)). The GSH concentration can be quantified by the ratio of FI$_{(\lambda_{em}=518nm)}$/FI$_{(\lambda_{em}=468nm)}$ which exhibits a linear relationship (1 μM to 15 mM) with the levels of GSH in both cancerous and normal cells. This is because the dye's fluorescence is obviously quenched by AuNPs in the nanospheres and recovered by the breakage of nanometal surface energy transfer (NSET). Then, after a 24 h incubation, it was determined how well nano-sensors were internalized into the HeLa and 293T cells. The nano-sensors successfully wrapped into the cells through endocytosis and displayed blue fluorescence and brighter green fluorescence, as opposed to the nanosensors that the cells did not endocytosis, which only display blue fluorescence. Due to the HeLa and 293T cells' elevated GSH levels, these can be attributed to the dye's (Fl–NH$_2$) fluorescence recovery, which also supports the viability of the nanosensors for recognition of the concentration of GSH inside cells.

Cobalt oxyhydroxide (CoOOH) nanosheets, which are typical hexagonally stacked two-dimensional transition metal nanomaterials, were also used to produce fluorescent polydopamine nanoparticles (PDANPs) in an easy and environmentally friendly way.[55] Surprisingly, the produced fluorescent PDANPs show superb chemical and photo-stabilities. However, when GSH was present, the GSH reduction on CoOOH nanosheets may reduce the fluorescence intensity of PDANPs (Fig. 3(d)), allowing the PDA NPs to be used as a label-free nanoprobe for GSH detection. When CoOOH nanosheets are available as
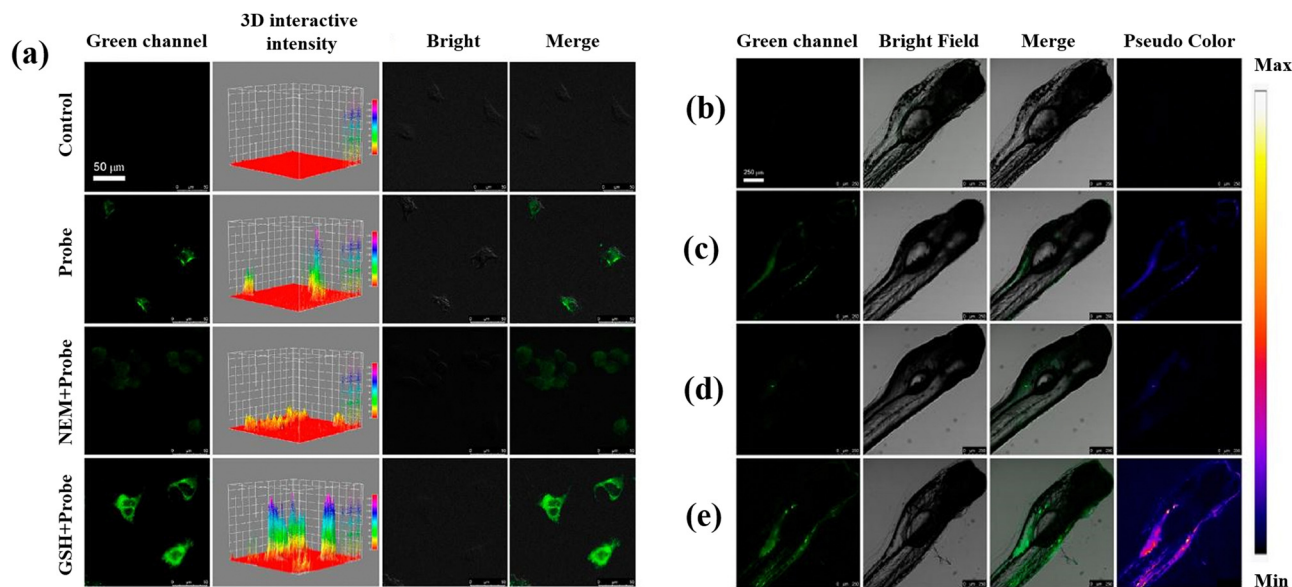
This journal is © The Royal Society of Chemistry 2024

J. Mater. Chem. B, 2024, **12**, 8285–8309 | **8293**

Fig. 4 (a) Untreated HeLa cells and HeLa cells incubated with DQ−CD@Pdots in different conditions. Fluorescence images of zebrafish: (b) untreated zebrafish, (c) zebrafish incubated with DQ−CD@Pdots for 3 h, (d) zebrafish incubated with NEM with the concertation of 100 μM, and (e) 100 μM GSH concertation for 10 min, and then incubated for 3 h with DQ−CD@Pdots. Reproduced from ref. 57 with the permission of American Chemical Society.

oxidants, dopamine may be quickly oxidized to its quinone derivative and subsequently self-polymerized into fluorescent PDA NPs. The CoOOH nanosheets oxidative ability towards dopamine can be destroyed in the presence of GSH by the GSH reduction (CoOOH + GSH + 2H$^+$ → Co^{2+} + GSSG + 2H$_2$O), which prevents the creation of fluorescent PDA NPs.

Highly N-doped carbonized polydopamine nanotubes (C-PDANTs) that resemble peroxidase were also prepared.[56] Dopamine's self-polymerization allowed PDA to first develop on the templates of sacrificial halloysite nanotubes (HNTs) as the sole precursor (Fig. 3(e)). For surface coating on almost all types of substrates, the simple dopamine self-polymerization to produce PDA in the presence of dissolved oxygen in a dilute alkaline solution has been extensively exploited.[108] Although the relevant substrate systems showed poor catalase-like, oxidase-like, and SOD-like activities, the N-doped C-PDANTs demonstrate substantial peroxidase-like activity and are capable of catalysing the chromogenic reaction of TMB and H$_2$O$_2$. N-doped C-PDANTs with peroxidase-like activity were used to detect GSH because GSH effectively quenched TMB oxidation.

Recently, the development of semiconducting polymer dots (Pdots), which provide special potential for biosensors and bioimaging in biological environments, has attracted a lot of attention.[109–111] Sun et al.[57] developed two-photon fluorescent hybrid Pdots made by grafting poly(styrene-co-maleic anhydride) (PSMA) with β-cyclodextrin (β-CD) and poly[(9,9-dioctylfluorenyl-2,7-diyl)-co-(1,4-benzo-{2,1′,3}-thiadiazole)] (PFBT). When GSH is present, the quinone-like structures (DQ) molecules on the Pdots surface are converted into the molecules of catechol, which inhibit PET and restore the Pdots' fluorescence and making possible to measure GSH. To assess the DQ−CD@Pdots' potential for imaging intracellular GSH,

HeLa cells were exposed to DQ−CD@Pdots, revealing their sensitivity to intracellular GSH (Fig. 4(a)). Moreover, DQ−CD@Pdots exhibited the sensitivity toward GSH concentration in the living zebrafish (Fig. 4(b–e)) proposing DQ−CD@Pdots probes have the ability to track variations in GSH concentrations in living bodies.

4. Metal−organic frameworks (MOFs) and covalent organic frameworks (COFs)

Metal−organic frameworks (MOFs) are a type of porous material formed by coordination of metal ions with ligands,[112] and they have a diverse framework as well as adjustable catalytic activity, making them a research hotspot for creating mimic enzyme materials.[113–115] MOFs have active sites with high density and uniform dispersion, and a large specific surface area is used for substrate adsorption and enrichment around the active site. Furthermore, MOFs can be used as natural enzyme carriers, allowing for high catalytic efficiency cascade reactions.[116,117] Over recent years, an increasing number of researchers have concentrated on the creation of new MOFs as mimetic enzyme materials. Metal−organic frameworks (MOFs) were produced by self-assembly of metal ions or clusters and organic bridging ligands with strong covalent connections.[59] MOFs sparked widespread interest not only for their large surface area, tuneable pore size, optical and chemical stability, and a slew of other excellent features, but also for their enormous application potential in a wide range of sectors.[118] Some examples include gas storage,[119] catalysis,[120] sensing of ions[121] or molecules,[122] and medication delivery.[123] Several research

8294 | J. Mater. Chem. B, 2024, 12, 8285–8309

This journal is © The Royal Society of Chemistry 2024

investigations have delved into examining the application of MOFs for detecting GSH.

Ce based metal–organic frameworks (Ce-MOF) was produced and utilized as a fluorescent probe to detect GSH,[58] through FRET between Ce-MOF and AuNPs, which leads to quenching the emission peak of Ce-MOF at 377 nm after the incorporation with AuNPs. The fluorescence of Ce-MOF was regained after the GSH addition to Ce-MOF/AuNPs due to the production of Au–S between GSH and AuNPs, resulting in the FRET suppression between AuNPs and Ce-MOF.

Using the hydrothermal method, Yang et al.[59] also developed a novel $[Co(L)(H_2O)_2]$ MOF possessing a 3D supramolecular structure produced by hydrogen bonding. Chemiluminescence was used to investigate the peroxidase-like activity, and it was discovered that MOF had a high affinity for the substrate. Catalytic mechanism investigation revealed that $[Co(L)(H_2O)_2]$ accelerated the breakdown of H_2O_2 to form reactive oxygen free radicals, resulting in an increase in the chemiluminescence signal. The inhibitory effect of GSH on the chemiluminescence signal of $[Co(L)(H_2O)_2]$ was utilized for the detection of GSH in cell lysates.

The utilisation of Cu_2O templates to produce Au@Cu-MOF nanocapsules, which have an embedded AuNPs layer and a Cu-MOF sandwich shell, was also reported for the GSH detection (Fig. 5(a)).[19] This method for detecting GSH has several noteworthy benefits: (a) the presence of Au^0 and Cu(I) bimetals in Au@Cu-MOF nanocapsules endows the sensor with exceptional conductivity and electrocatalytic activity as well as a good microenvironment for Cu(I); (b) the addition of Cl^- can cause CuCl to undergo solid-state electrochemistry; however, GSH could cause the electroactive CuCl conversion to a complex of nonelectroactive Cu–GSH having a larger signal reduction, which facilitates the direct GSH tracking; (c) the obtained Au@Cu-MOF nanocapsule-modified electrode showed steady and precise solid-state CuCl current at a very low potential of about 0.06 V, which can rule out the interferences of potential redox from background electroactive chemicals. Additionally, the natural frameworks of Cu-MOF could stop Cu(I) from oxidizing and AuNPs from aggravating in order to maintain the sensor's long-term stability.

A new sensing platform was proposed for the quantification of GSH using 3D Cu-tetrakis(4-carboxyphenyl)porphyrin (Cu-TCPP) nano-flowers (NFs) functionalized with Ag nanoparticles, followed by the modification of the electrode surface with Ag/Cu-TCPP MOF NFs (Fig. 5(b)).[124] Because of the activated electrode surface adsorption and the production of the complex of Cu(II)–GSH, GSH exhibits a lower potential of oxidation and a greater current of oxidation at Ag/Cu-TCPP/GCE compared to
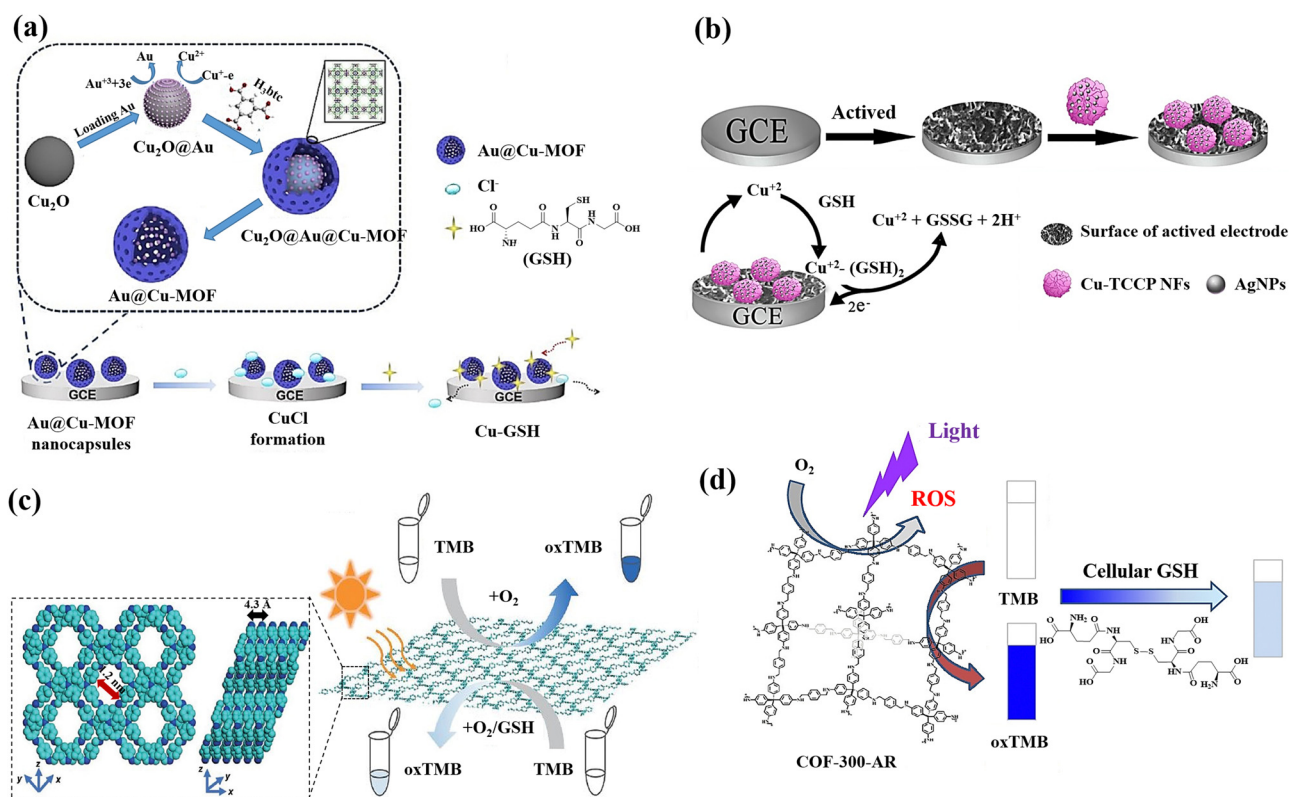

Fig. 5 (a) Preparation of Au@Cu-MOF nanocapsules and graphical representation of the sequential steps of the Au@Cu-MOF nanocapsule-modified electrode involving Cl^- ion electrochemical reactions first, followed by GSH,[19] (b) the fabrication of the electrochemical sensor using Ag/Cu-TCPP nanocomposites and glassy carbon electrodes (GCEs) for the GSH detection based on Possible electrochemical oxidation mechanism of GSH,[124] (c) Top and side view of the energy-minimized models of TTPA-COF and the schematic illustration of GSH detection using TTPA-COF,[20] (d) schematic illustration of the GSH recognition in cell lysate during visible light irradiation relying on the oxidase-mimicking activity of COF-300-AR[61] reproduced with the permission of Elsevier, American Chemical Society, and Springer Nature.

This journal is © The Royal Society of Chemistry 2024

J. Mater. Chem. B, 2024, **12**, 8285–8309 | **8295**

the bare glassy carbon electrode.[125] The suggested GSH sensor exhibits a broad linear range and a low limit of detection, as well as a potent anti-interference ability thanks to the synergistic impact the huge unique Cu-TCPP NFs surface area and the Ag NPs high electrical conductivity.

Covalent organic frameworks (COFs) are also a new class of covalently bonded porous crystalline polymers.[126] The extensive use of COFs as a platform for photoinduced catalysis depends on their array framework, high crystallinity, configurable band gaps, and appealing optoelectronic performances.[127] For active sites like metal organic frameworks, they can disseminate and customize the hydrophobic spatial environment.[127,128] However, the fabrication of nanozyme was severely constrained by the poor MOF stability in the aqueous phase.[129] Fortunately, COFs have proven to be an excellent supporting matrix as stable porous materials.[130] The functional groups found in COFs may function as Lewis acid-bases to aid in the transfer of protons or electrons during catalytic reactions.[131] Particularly, COFs with amines and triazine rings have the ability to closely resemble the amino acid residues found in naturally occurring enzymes.[132] Regarding the GSH sensing, COFs has also attracted researchers' attentions as promising nanomaterial for detecting GSH.

A donor–acceptor two-dimensional (2D) COFs (designated as Py–TT COFs) was developed and used as a light-responsive oxidase mimic for the GSH detection. The donor was 1,3,6,8-tetrakis(4-aminophenyl)pyrene (Py), and the acceptor was thieno[3,2-b]thiophene-2,5-dicarbaldehyde (TT).[60] Photoabsorption capacities in the crystalline Py–TT COF were efficiently improved by organized Py and TT arrays, narrow band gaps, and easier charge separation and transportation. The photoactivated donor–acceptor Py–TT COF with enzyme-like catalytic capabilities could serve as a probe for quick colourimetric detection of GSH in the presence of 3,3′,5,5′-tetramethylbenzidine (TMB). The illuminated Py–TT COF demonstrated a good light-responsive oxidase-like activity for the TMB oxidation, and the addition of GSH led to the oxidized TMB reduction, resulting in the conversion of the blue colour into colourless, leading to the colourimetric method for GSH detection.

A unique ultrathin nanosheets,[20] dubbed the nanosheets of TTPA-COF, employing flexible photoactive N,N,N′,N′-tetrakis(4-aminophenyl)-1,4-phenylenediamine (TAPPDA) and N,N,N′,N′-tetrakis(4-formylphenyl)-1,4-phenylenediamine (TFPP) was designed and fabricated (Fig. 5(c)). The TAPPDA and TFPPDA incorporation into the TTPA-COF framework can significantly diminish interlayer contacts, leading to the efficient direct fabrication of ultrathin TTPA-COF nanosheets with a good yield. Upon light irradiation, the TTPA-COF nanosheets as produced demonstrate strong binding affinity towards the TMB substrate in addition to their ability to simulate an oxidase activity. Further, because GSH could hinder the TTAP-COF nanosheet-based oxidase-like nanozyme catalytic activity toward the TMB oxidation, a colourimetric sensor with high selectivity and sensitivity for GSH recognition with the limit of detection of 0.5 μM is proposed.

A COF-300-AR,[61] which demonstrated strong enzyme-mimicking activity by emitting a purple light at a wavelength of 400 nm, was produced for the purpose of GSH sensing (Fig. 5(d)). The typical substrates 2,2′-azino-bis(3-ethylbenzothiazoline-6-sulfonic acid) (ABTS) and 3,3′,5,5′-tetramethylbenzydine (TMB), whose function was similar to that of the oxidase, were oxidized by COF-300-AR under the stimulus of purple light. The photostimulated COF-300-AR demonstrated exceptional versatility, simple light control, and durability in contrast to natural oxidase. The system of TMB-COF-300-AR was additionally employed as a platform of colourimetric for the GSH assessment in cell lysates.

The luminous COFs formed thanks to the Schiff base reaction between melamine and terephthalaldehyde was also developed to detect GSH.[62] It was discovered that MnO_2 nanosheets efficiently quench the fluorescence of COFs, and the processes involved are IFE and the static quenching effect (SQE). The subsequent reduction of MnO_2 to Mn^{2+} ($2GSH + MnO_2 + 2H^+ \rightarrow GSSG + Mn^{2+} + H_2O$), leading to the fluorescence recovery of COFs, can be triggered by the GSH addition to the COF–MnO_2 nanosheet composite.

A novel peroxidase-like nanozyme called FeS_2-encapsulated SNW-1 (FeS_2@SNW-1) was created[63] by using hydrothermal and solvothermal processes. The hydrophobic porous SNW-1's protective effect on the FeS_2 active centre allowed for the durability and versatility of the nanozyme as a potential fluorescence GSH probe, as well as electrochemical dual-signal capability. In this sensing system, FeS_2@SNW-1 nanozyme accelerated the hydroxyl radical (•OH) production from H_2O_2, and O-phenylenediamine (OPD), a chromogenic substrate, was subsequently further oxidized (Fig. 6(a)). The OPD's oxidation product exhibits notable electrochemical activity and fluorescence. After addition of the GSH to the sensor system, the GSH molecules react with •OH and hampers the OPD oxidation reaction resulting in the decline of the fluorescence intensity and the current drop. FeS2@SNW-1 nanozyme's strong catalytic performance allowed for the dual-signal GSH recognition in cell lysates. FeS_2@SNW-1 nanozyme's strong catalytic performance allowed for the dual-signal GSH recognition in cell lysates. To provide the sensing system with uncomplicated and easily transportable attributes, a fluorescence test strip for visually quantifying GSH was also created (Fig. 6(b)).

5. Quantum dots (QDs)

QDs are semiconductor nanostructures that are 1–20 nm in size and have intriguing photo-physical and photochemical characteristics.[133] Due to the quantum confinement effect, which causes their photoluminescence to be size- and composition-dependent, QDs have special absorption and emission properties as a result of their small size.[134] QDs are highly suitable for sensing applications due to their unique chemical properties. The quantum confinement effect in QDs results in discrete energy levels and size-dependent optical and electronic characteristics, providing precise control over their
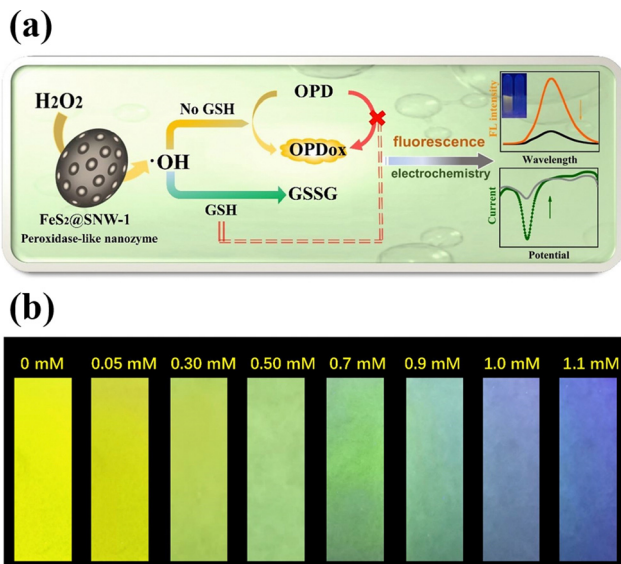
8296 | J. Mater. Chem. B, 2024, 12, 8285–8309

This journal is © The Royal Society of Chemistry 2024

(a)

(b)

Fig. 6   (a) Schematic of a FeS2@SNW-1 biosensor for detection of GSH *via* dual-signal analysis, (b) the fluorescence test paper for GSH detection under UV light of 365 nm. Reproduced from ref. 63 with the permission of Elsevier.

behavior.[135] Their surfaces can be functionalized with various ligands and functional groups, enhancing specificity and sensitivity to target molecules. QDs exhibit efficient charge transfer, strong and tuneable photoluminescence, and high quantum yield, leading to bright and stable fluorescence signals.[136] They are chemically stable under various conditions, ensuring consistent performance, and can be engineered for multifunctionality, such as incorporating magnetic or catalytic properties. It is feasible to achieve fluorescence with the capacity to tune it across the entire spectral range, from ultraviolet (UV) to near-infrared, by varying composition and size.[137] They are one of possible options for optical sensor applications because they have a broad absorption band and a compact fluorescence emission profile with the strong photobleaching resilience.[138,139] Due to the excellent physical and chemical properties of these nanomaterials, researchers have focused on utilizing QDs for GSH detection, making them promising candidates in this field.

A molybdenum disulphide quantum dot/manganese dioxide nanosheet (MoS_2 QDs/MnO_2) was developed for the GSH detection.[64] MnO_2 nanosheets reduced the fluorescence of MoS_2 QDs due to the inner filter effect (IFE) and static quenching effect (SQE) (Fig. 7(a)). The fluorescence of MoS_2 QDs is subsequently restored by the reduction of MnO_2 that occurs as a result of the addition of GSH, which also causes the disintegration of MnO_2 nanosheets. In addition, the MnO_2 nanosheets' colour shift was caused by GSH's reduction of the MnO_2 nanosheets leading to the development of double-signal sensing system (fluorometric and colourimetric technique).

A nanoprobe based on MXene $N-Ti_3C_2$ quantum dots ($N-Ti_3C_2$ QDs) was prepared for detection of intracellular GSH.[65] Based on non-radiative electron–hole annihilation, the ferric iron (Fe^{3+}) served as the quencher and the $N-Ti_3C_2$ QDs as the

fluorescence reporters (Fig. 7(b)). The reduction of Fe^{3+} to Fe^{2+} by intracellular GSH resulted in a recovery of the fluorescence intensity in the cell lysates, allowing for the intracellular GSH detection.

An ''on–off–on'' fluorescence sensor for GSH recognition was created using cryogenic-mediated liquid-phase exfoliation to construct bifunctional VOx QDs with fluorescence and redox capacity.[66] The VOx QDs as-prepared displayed blue emission and served a reductive function. The internal filtering effect (IFE) between VOx QDs and MnO_2 nanosheets caused the fluorescence of VOx QDs to be quenched with the addition of MnO_4. However, the quenched fluorescence of VOx QDs could be restored with the GSH addition, which can breakdown MnO_2 nanosheets.

Orange-emissive sulphur (S)-doped organosilica nanodots (referred to as S-OSiNDs) were prepared using a solvothermal approach and the urea, bis[3-(triethoxysilyl)propyl]tetrasulphide, and citric acid as precursors.[67] The S-OSiNDs displayed hydrophilicity and good photoluminescence stability and found that metal ions Cu^{2+} could significantly reduce the S-OSiNDs fluorescence (Fig. 7(c)). Due to the great preference for GSH for the creation of the strong Cu–S bond, the metal ions were removed from the S-OSiND's surface when GSH was added to the suspension of S-OSiNDs-Cu, leading to the S-OSiNDs-Cu disassembly to S-OSiNDs and fluorescence recovery.

The preparation of sulphur quantum dots (H-SQDs), which identified with an enhanced emission of anodic electrochemiluminescence (ECL) in an aqueous solution, was described[18] using a top-down technique and a post-synthetic etching strategy (Fig. 7(d)). In-depth analyses showed that the reduction in size for intrinsic luminosity, the extremely treated surface, and the improved capabilities of injection/transfer of charge after the post-synthetic hydrogen peroxide etching were responsible for the greatly improved ECL performances of H-SQDs. The *in situ* anchoring of H-SQDs on MnO_2 nanosheets created an architecture of ECL-RET system, and the nanocomposite displayed a nearly quenched ECL response, indicating a ''signal-off'' state for the sensitive and focused recognition of GSH with limit of detection of 35 nM and linear range of 0.05 to 5.0 µM. The H-SQDs@MnO_2 nanocomposite ECL recovery was observed after the GSH addition due to the reduction of MnO_2 NSs to Mn^{2+} and recovering the H-SQDs fluorescent properties.

A ratio-sensing platform for the detection of GSH was built using WS_2 quantum dots (QDs) as fluorescent signals and MnO_2 nanosheets as sources of second-order scattering (SOS) signals[68] The IFE to WS_2 QDs was inhibited when the MnO_2 nanosheets' distinctive absorption peak vanished, which led to the recovery of WS2 QDs' fluorescence. The size of the MnO_2 nanosheets shrinks as a result of GSH's breakdown, which lowers the system's SOS leading to the ratiometric detection of GSH using the fluorescence and SOS dual signal response.

A CdTe QD probe by joining a quencher, polynitroxylated albumin (PNA) made by covalently tagging human or bovine serum albumin with several nitroxides, 4-acetamido-TEMPO (AcTPO), was created for the preparation of CdTe–PNA.[69] The photoinduced or surface-trapped electron transfer mechanism
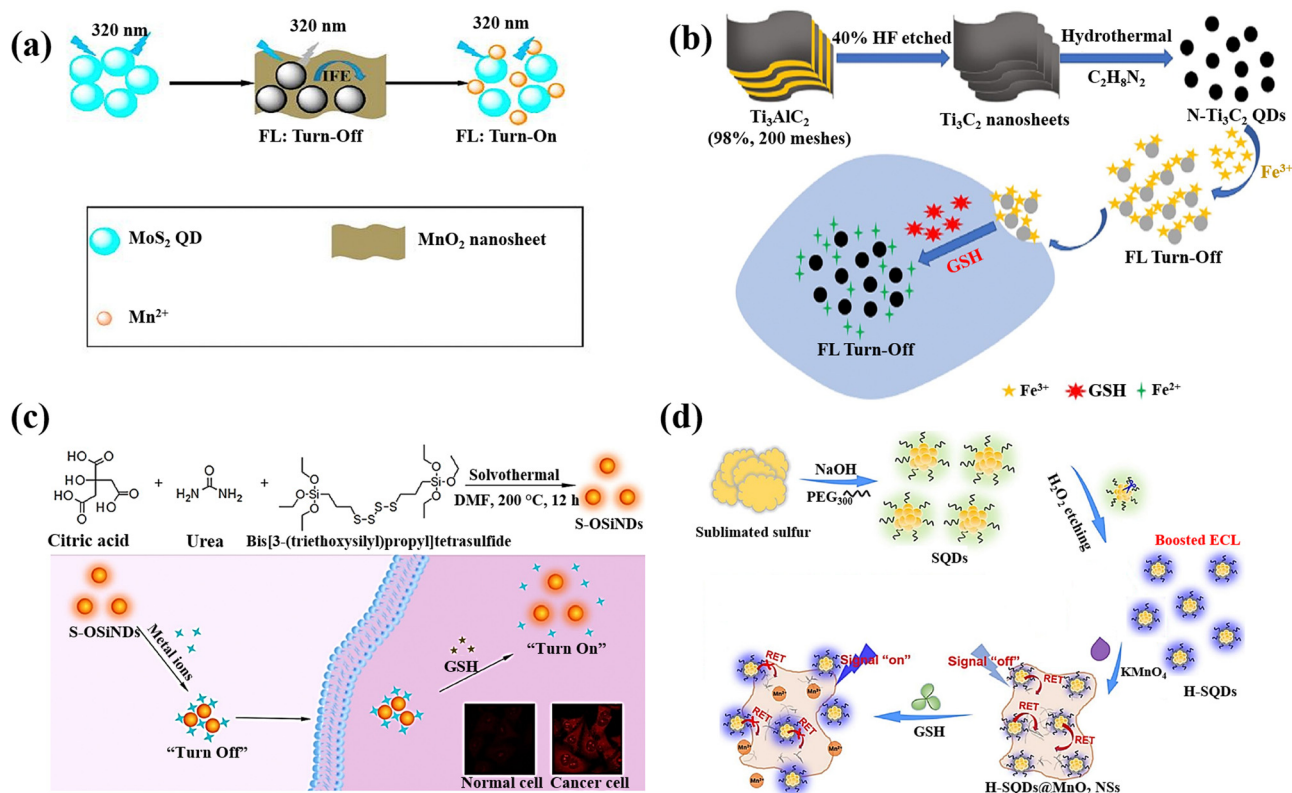
Fig. 7 (a) Double-signal MoS_2QDs/MnO_2 nanoprobe schematic depiction for detection of GSH,[64] (b) $N-Ti_3C_2$ QDs/Fe^{3+} probe preparation and GSH detection,[65] (c) The production of S-OSiNDs and their use in cancer/normal cell distinction and GSH detection based on the S-OSiNDs' "on–off–on" fluorescence response feature,[67] (d) H-SQD synthesis and the "off–on" ECL-RET platform design for the detection of GSH[18] reproduced with the permission of Elsevier and American Chemical Society.

from CdTe to polynitroxides on PNA is responsible for the dynamic quenching. Using the concept of PNA-induced quench of CdTe PL and recovery with the GSH addition, CdTe–PNA nanocomposites were employed for the detection of GSH, and albumin acts as a bridge between nitroxide free radicals and CdTe QDs, increasing the biocompatibility of the nanocomposites and decreasing QD cytotoxicity.

A black phosphorus quantum dot (BPQD) nanocomposite wrapped in manganese dioxide nanosheets (BPQDs@MnO_2)-based imaging and determination approach for GSH was also presented.[70] Fluorescence resonance energy transfer (FRET) induces the fluorescence quenching of BPQDs@MnO_2, and in the presence of GSH, reactivation occurs (Fig. 8(a)). BPQDs@MnO_2 exhibited a strong fluorescent imaging signal in three different types of tumour cells, while normal cells displayed a weak signal; furthermore, the incubation of BPQDs@MnO_2 and A549 tumour cells (Fig. 8(b)) demonstrated a GSH-activated MRI imaging signal.

6. Gold and other metal-based nanomaterials

AuNPs can be a remarkable nanomaterial to generate innovative nano-sensors because of their excellent electrical, optical,

chemical, and catalytic properties, as well as easy preparation, strong distance dependent optical features, high extinction coefficients, high surface-to-volume ratio, and good biocompatibility, in addition to characteristic of suitable surface functionalization.[140,141] They exhibit surface plasmon resonance (SPR), which provides strong and tuneable optical absorption and scattering, making them highly sensitive to environmental changes.[142] The surface of AuNPs can be easily functionalized with various ligands and biomolecules through strong Au–S bonds, enhancing their selectivity and sensitivity. AuNPs are chemically stable and resist oxidation, ensuring reliable performance. Additionally, AuNPs have catalytic properties that can amplify signals in certain sensors and a high electron density that improves electrochemical sensing.[143] These properties, along with their ease of synthesis and versatile functionalization, make gold nanoparticles highly effective for diverse sensing applications. The most effective analytical techniques for detecting biomolecules, including amino acids, peptides, proteins, nucleic acids, and enzymes are colourimetric and electrochemical uses of AuNPs in sensing.[144] Recently, there has been a notable application of gold nanoparticles, particularly emphasizing the utilization of surface-modified variants of these nanomaterials, in the detection of GSH.

An approach based on the creation of a colourimetric sensor using AuNPs was designed for the GSH detection by adjusting
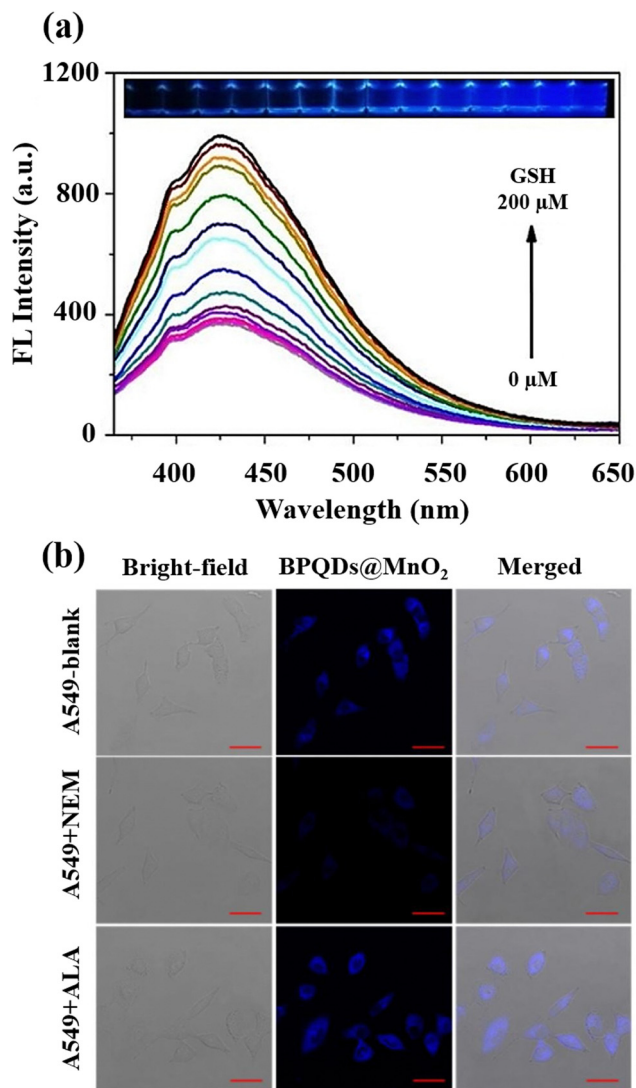
8298 | J. Mater. Chem. B, 2024, 12, 8285–8309

This journal is © The Royal Society of Chemistry 2024

Fig. 8   (a) BPQDs@MnO$_2$ fluorescence spectra at various GSH levels and the accompanying images under 365 nm UV light, (b) A549 cells fluorescence imaging incubated by BPQDs@MnO$_2$ with the NEM and α-lipoic acid (ALA) addition. Scale bar (20 μm). Reproduced from ref. 70 with the permission of Elsevier.

the pH to 5.8 in order to GSH sensing based on the anti-aggregation of AuNPs (Fig. 9(a)).[71] Electrostatic repulsion between the negatively charged sodium citrate coatings keeps the AuNPs stable in aqueous solution. 2-Mercapto-1-methylimidazole (MMI) can attach to the surface of AuNPs due to the potent covalent association of Au and SH resulting in the aggregation AuNPs and a colour shift from red to blue. Nonetheless, when both MMI and GSH are in AuNPs aqueous dispersion, the thiol of GSH reacts with AuNPs to form Au–S bonds, preventing MMI from attaching to AuNPs surface. As a result, it can be affirmed that the mechanism is the competition of GSH over MMI rather than GSH binding the excess empty surface of the MMI-bound AuNPs and causing dispersion, and the colour is altered from blue to red, leading to the calorimetric GSH recognition.

Depending on the quenching effect of S$_2$O$_8$$^{-2}$ against Au–Ag bimetallic NCs, Zhai et al.[21] developed a fluorescence sensor for GSH sensing utilizing bovine serum albumin (BSA) as a protective and reducing agent for the production of Au–Ag bimetallic NCs with increased fluorescent intensity. Due to GSH's great reducibility to S$_2$O$_8$$^{-2}$, the fluorescent was restored while it was present, and the recovered fluorescent intensity relied on the GSH content (Fig. 9(b)). The Au–Ag bimetallic NCs fluorescence emission in the presence of various S$_2$O$_8$$^{-2}$ concentrations confirmed how strong oxidation capability of S$_2$O$_8$$^{-2}$ s can significantly reduce the fluorescent intensity of Au–Ag bimetallic NCs.

The issues were also addressed by presenting a lateral flow plasmonic biosensor (LFPB) comprised of gold-viral biomineralized nanoclusters (AuVCs) and lateral flow strip for quick GSH detection with the naked eye.[72] In the presence of AuVCs, the levels of GSH regulates the formation of AuNPs (Fig. 9(c)) and produces coloured patterns in the LFPB detection region, which are then automatically evaluated by a smartphone app to detect the GSH levels. In this study, the plasmid vectors encoding the genome of the Q coat protein (QCP) were expressed, and the QCPs would self-assemble into virus-like particles (VLPs). When the VLPs are combined with TMB/H$_2$O$_2$ solution, there is no response, indicating that the catalytic capacity results from the gold cluster in VLPs rather than the viral coat proteins. The produced AuVCs were used as a template, allowing the growth of AuNPs on their surface as a plasmonic signal for determining GSH content via AuNP growth control because GSH would collapse the AuVCs in the suggested technique to decrease the creation of AuNPs.

Using the peroxidase-like activity of gold nanocrystals stabilized with GSH (GSH–AuNCs), a straightforward method was provided for the cellular GSH level detection using colourimetric approach.[73] The peroxidase substrate 3,3′,5,5′-tetramethylbenzidine (TMB) can be oxidized by the AuNCs in the H$_2$O$_2$ presence to form a blue-coloured solution; nevertheless, GSH can effectively suppress this reaction, causing the blue colour to fade. Depending on this, a quick and simple method for colourimetrically detecting GSH with the human eye using the proposed method.

A 3D-printed integrated smartphone-sensing platform for the visible, quick, on-the-spot GSH detection in human serum, in particular in low-resource settings was also developed (Fig. 10).[74] In order to create a fluorescent paper test, a blue fluorescent carbon dots (CDs) and AuNCs were used as the probe solution. As a responsive unit, the orange emissive AuNCs with strong fluorescence emission were quenched whereas the blue fluorescence remained constant in the presence of copper ion (Cu^{2+}). Due to the greater affinity between SH of GSH and Cu^{2+}, which has a wide and unique colour change from blue to purple to orange, the orange fluorescence is gradually improved with the addition of GSH. Then, a Colour Recognizer APP loaded on the smartphone could do quantitative detection by recognizing the relevant red (R), green (G), and blue (B) values. The single-colour probe's emission response (AuNCs–Cu^{2+}) was also investigated to GSH

This journal is © The Royal Society of Chemistry 2024
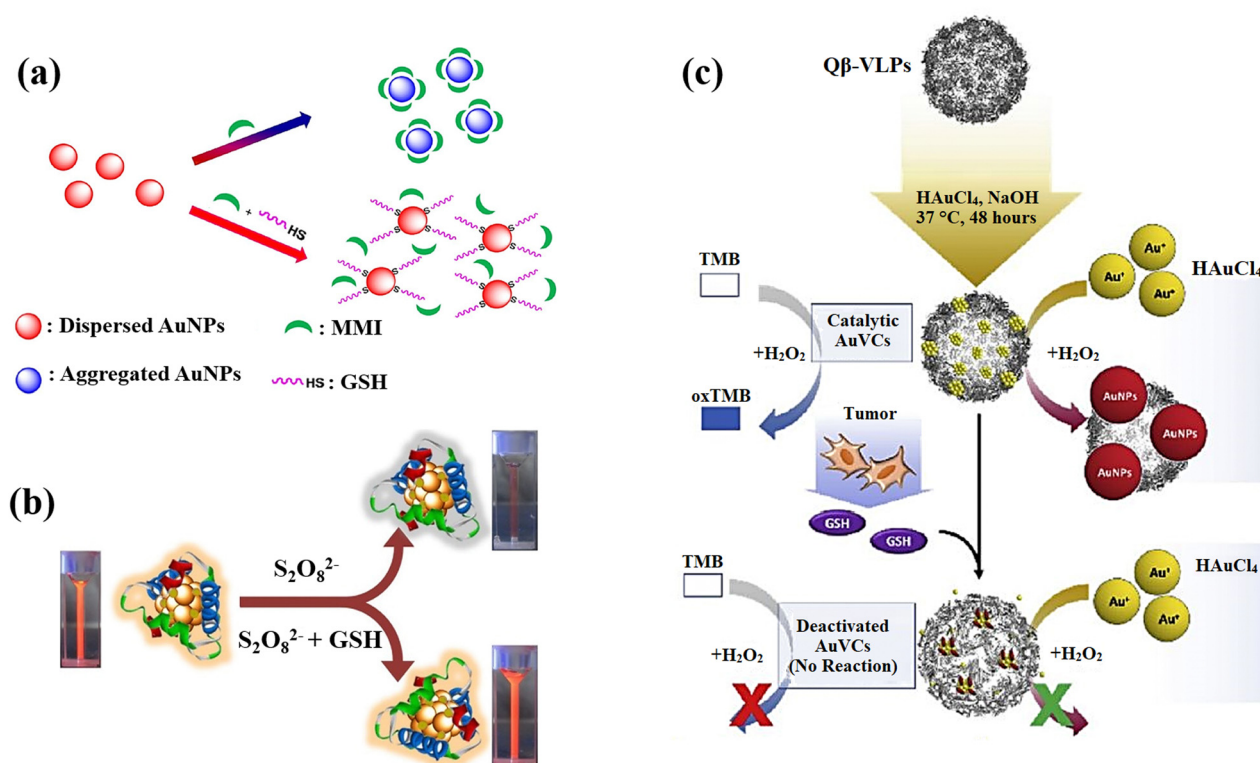
J. Mater. Chem. B, 2024, 12, 8285–8309 | 8299

Fig. 9 (a) Schematic illustration of AuNPs' anti-aggregation generated by GSH using of 2-mercapto-1-methylimidazole (MMI) as aggregation agent,[71] (b) GSH detection scheme that uses the quenching effect in relation to Au–Ag bimetallic NCs,[21] (c) the scheme design and processes for preparation of AuNCs and GSH detection. For production of AuNCs, HAuCl$_4$ and NaOH were co-incubated with Qβ-VLPs. In the presence of HAuCl$_4$ and H$_2$O$_2$, the generated AuVCs, which are GSH sensitive, may catalyze the creation of AuNPs. The reduced catalytic ability resulting from AuVC deactivation led to a low yield of AuNP production[72] reproduced with the permission of Elsevier.

in order to contrast its performance with that of the ratiometric composite probe.

More recently, the exploration of other metallic nanomaterials rather than AuNPs has attracted significant attention in the realm of biomolecule sensing.[145,146] While AuNPs have demonstrated remarkable properties for biosensing applications, the diverse characteristics of other metallic nanomaterials offer unique advantages exhibiting promising features such as tuneable surface plasmon resonance, catalytic activities, and distinct electrochemical behaviour, which are pivotal for achieving superior performance in biomolecule sensing.[147–149] This expanding frontier in nanomaterial utilization underscores the rich potential for diversifying the toolbox of sensing platforms, thereby broadening the scope and efficacy of biomolecular detection, particularly in the context of GSH sensing.

Two-dimensional (2-D) nanomaterials, such as transition metal dichalcogenide MoS$_2$, were synthesized employing a hydrothermal approach, which has a large surface area, morphology control, and good flexibility during the preparation, giving them unique characteristics and a strong substrate selectivity for nanozymes.[75] Due to a synergistic effect, it was discovered that Fe-doped MoS$_2$ (Fe–MoS$_2$) had higher catalytic activity than other metal ions, and with percentage doping reaching a saturation level at 10%, it was discovered that there is a synergistic improvement in the Fe–MoS$_2$ peroxidase

mimetic activity. By means of its suppressive influence peroxidase mimetic activity for the oxidation of TMB, producing blue colour contrast, Fe–MoS$_2$ has been used for GSH detection (limit of detection: 0.577 μM).

NaYbF$_4$@CaF$_2$ a new category of core–satellite up-conversion nanoparticles (UCNPs) was presented for the GSH detection (Fig. 11(a)).[22] In this study, a sequential injection method for managing the CaF$_2$ shell deposition on the core nanoparticles was developed and determined the crucial significance of directed connection throughout the fabrication of the satellite-core structure by analyses of the morphological change over time and as a function of injection rate. A benefit of the core–satellite UCNPs for surface derivatisation is their superior adsorption capability in the porous shell, and an energy transfer-based biosensing system was developed using MnO$_2$ nanosheets coated on the α-NaYbF$_4$@CaF$_2$ core–satellite UCNPs, which the MnO$_2$-coupled UCNPs offer a turn-off FRET probe that detects recovered emissions when introducing GSH as a reducing agent resulting in the GSH detection.

MXenes, a newly developed 2D conductive material derived from transition metal carbides and nitrides, has been extensively researched due to its potential to propel the field of low-dimensional materials technology.[150] Due to its exceptional mechanical and electrical properties, this new class of materials is valuable in a variety of fields. The past several years have
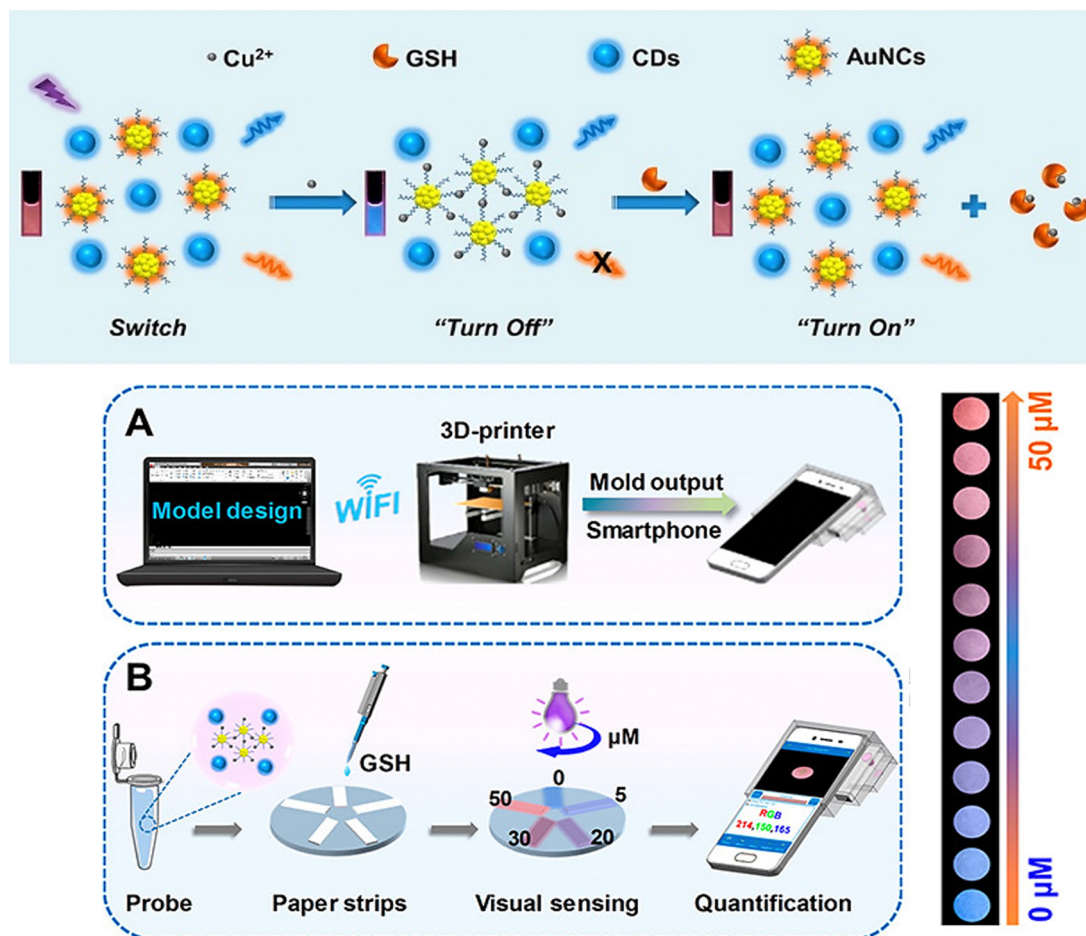
Fig. 10 (a) Schematic demonstrating the steps involved in producing the ratiometric probe and the GSH detection principle using a blue fluorescent carbon dots (CDs) and AuNCs. (b) Designing a smartphone detecting system with 3D printing. (c) GSH quantification and visual detection along with a collection of fluorescence photos taken with a smartphone camera and various GSH concentrations addition. Reproduced from ref. 74 with the permission of American Chemical Society.

seen a significant improvement in MXene-based sensor technology due to these essential features that make MXenes a viable alternative sensor material.[151] The development of an MXene@NiFe-LDH nanohybrid was also reported for the GSH detection since the prepared nanohybrid applied as the effective catalyst for the oxidation of TMB producing a blue colour in the presence of H_2O_2 with a blue hue, which fades very fast when GSH is added to the same solution (Fig. 11(b)).[76] The negatively charged surface of MXene (because of the presence of rich surface functional groups) used as a platform for LDH loading is responsible for the enhancement of metal ions anchoring and LDH nucleation. Furthermore, the high electrical conductivity would increase electron transport during the detection of GSH. The nanocatalyst's mechanism was also described as a heterogeneous Fenton-like catalytic reaction that produces hydroxyl radicals ($^{\bullet}OH$) due to the breakdown of acidified H_2O_2, whilst a blue product that forms when TMB is oxidized serves as a bridge to expedite electron transfers between TMB and H_2O_2.

A method for creating mixed-valence-state cobalt (MVSC) nanomaterials was applied using a self-sacrificial template which was $Co_3(BTC)_2 \cdot 12H_2O$ with a clearly specified structure.[77] It was made utilizing a high-temperature solution-phase manufacturing process. Co^{2+} ions in $Co_3(BTC)_2 \cdot 12H_2O$ were partially oxidized by $H_2O_2/NaOH$ at room temperature, resulting in MVSC nanomaterials with incredibly high specific surface areas and exceptional oxidase-like catalytic activity. It is interesting to note that altering the Co^{2+}/Co^{3+} ratio allowed for fine-tuning of MVSC's catalytic activity, and due to the GSH antioxidant ability, a simple and sensitive colourimetric sensor was developed for GSH detection (Fig. 11(c)).

7. Silicon oxide-based nanomaterials

Given their appealing properties, such as their large surface area, tuneable pore sizes, high pore volume, abundance of outer/inner surface chemistries, and inherent biocompatibility, silica-based nanomaterials have been the subject of numerous studies in the development of biomedical utilizations, including tissue engineering, biological imaging, controlled/
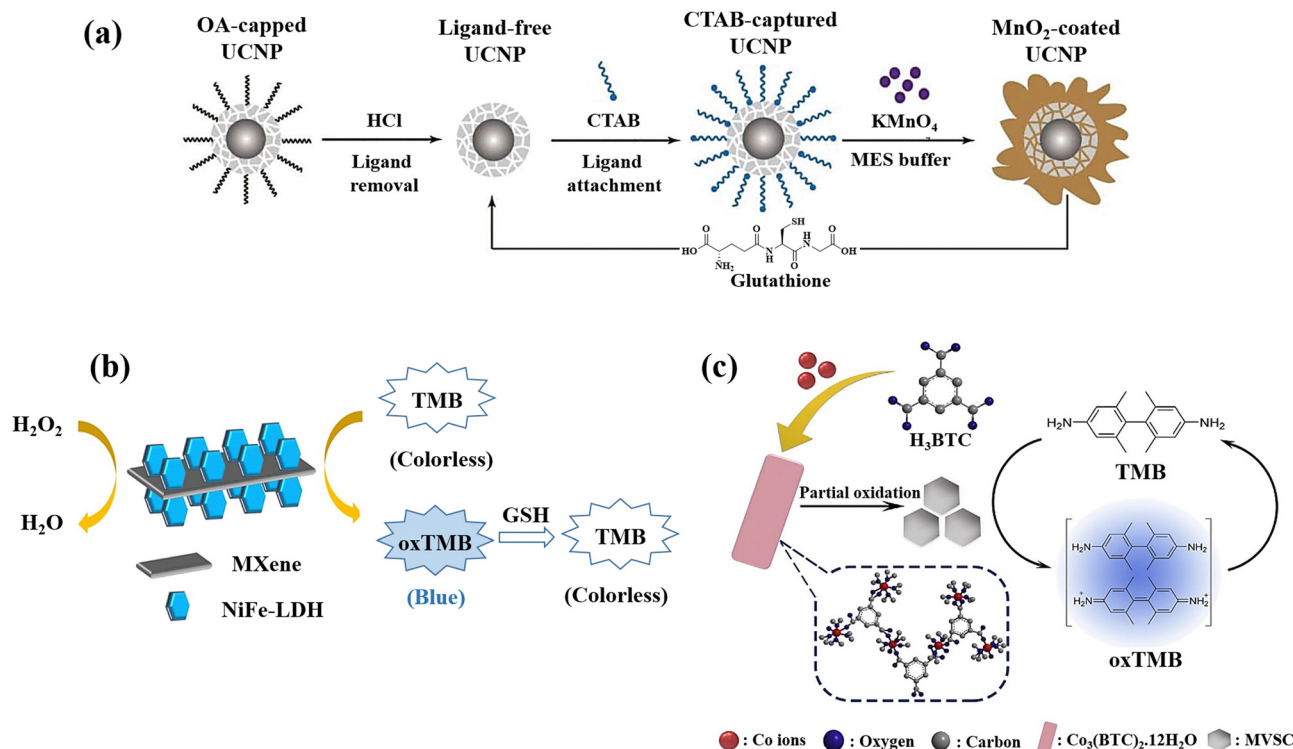
This journal is © The Royal Society of Chemistry 2024

J. Mater. Chem. B, 2024, **12**, 8285–8309 | **8301**

Fig. 11 (a) Graphical representation of surface alteration and GSH recognition by employing the α-NaYbF4:Tm (1%)@CaF$_2$ core–satellite UCNPs.[22] (b) Colourimetric GSH detection *via* MXene@NiFe-LDH nanocatalyst.[76] (c) Diagram of preparation of Co$_3$(BTC)$_2$·12H$_2$O and mixed-valence-state cobalt (MVSC), as well as colourimetric sensor for GSH detection[77] reproduced with the permission of Royal Society of Chemistry, American Chemical Society, and Elsevier.

sustained drug administration, and biosensors.[152–154] For instance, the large surface area of this type of nanomaterial makes it suitable to immobilize the sensing agents on both the outer surface and inside of pores, resulting in quick responses and optical detection through material layers.[155] Porous silicon can be created through several methods, such as physical, physicochemical, chemical, and electrochemical processes.[156] During the silicon etching procedure, it is possible to achieve a range of pore sizes from a few nanometers to several micrometers. The interest in utilizing porous silicon as a sensing material stems from its high surface reactivity and the vast surface area of its porous formations.[157] Additionally, the structure of porous silicon is crucial for sensing applications, as the diameter of the pores determines the size of the particles that can be trapped within them.[158] Due to these special features, a broad range of silica-based nanomaterials structures have been developed and explored for the production of biosensors, such as those that detect cocaine,[159] glucose,[160] nucleic acids,[161] H$_2$O$_2$[162] and NO$_2$,[163] and several types of anions.[164] In the context of GSH sensing, several research studies have been reported for the preparation and evaluation of silica-based nanomaterials for the GSH detection purposes.

A silica nanoparticles (SiNPs) functionalized with amine groups was applied to fabricate a new glassy carbon (GC) electrode, and due to a synergistic surface effect brought on by the integration of graphene quantum dots (GQDs) over SiNPs, the manufactured GQDs-SiNPs/GC electrode exhibited electrocatalytic activity towards GSH recognition in the biological environment at low voltage.[78] The voltammetry and amperometry tests were applied to evaluate the electrochemical functionality of the glassy carbon electrode improved with GQDs-SiNPs. To produce GQDs, citric acid was reduced in the first phase using an insufficient pyrolysis technique. Then, using tetraethyl orthosilicate (TEOS) and ethanol as a solvent, silica nanoparticles were produced. The cyclic voltammetry (CV) peak current values at the GQDs-SiNPs/GC electrode are respectively 3.98, 4.84, and 8.10 times greater than those at the SiNPs/GC, GQDs/GC, and bare GC electrodes suggesting that the addition of GQDs has improved the electrocatalytic activity of SiNPs, increasing both the specific surface area and the electric conductivity, leading to an improved ability to detect GSH.

A label-free MnO$_2$ nanosheet assisted TPE3-silica nanospheres (SiO$_2$ NPs) nanoprobe was designed Zhang *et al.*[23] for GSH detection, and the anionic tetraphenylethylene derivative 1,2-bis[4-(3-sulfonatopropoxyl)-phenyl]-1,2-diphenylethene sodium salt (TPE3) was created and used as the aggregation-induced emission (AIE) active probe. As a fluorescent reporter, TPE3 can aggregate on the surface of amino-functionalized SiO$_2$ NPs to generate AIE-SiO$_2$ NPs, which emit intense fluorescence (Fig. 12(a)). Due to electrostatic repulsion and steric hindrance between TPE3 and MnO$_2$ nanosheets having

8302 | *J. Mater. Chem. B*, 2024, **12**, 8285–8309

This journal is © The Royal Society of Chemistry 2024

negative charge, the synthesis of MnO_2–SiO_2 NPs nanocomposite could not lead to the TPE3 aggregation on the SiO_2 NPs surface. The dissociation of the MnO_2 by GSH, however, has the possibility of releasing the coated amino-functionalized SiO_2 NPs and expose their positive charges. Consequently, the limitation of TPE3's intramolecular rotation in the aggregated state allowed it to aggregate on the uncoated amino-functionalized SiO_2 NPs to produce AIE-SiO_2 NPs, which thereafter generate intense fluorescence showed a linear relationship to the GSH levels.

In another research study, mesoporous silica nanoparticles (MSN) of around 100 nm were chosen as a support and were functionalized with disulphide-containing oligo(ethylene glycol) groups that function as molecular gates after surface modification of MSN using safranin O as a dye (Fig. 12(b)).[79] The disulphide bond's selective reduction by GSH, which was anticipated to lead to opening pores and releasing dye, is the foundation of the signalling theory. The promising results encouraged the research group to quantify GSH in a more complicated system, choosing human serum, which exhibited the high recovery ratios ranging from 92 to 107 percent in a highly competitive environment like human serum.

Using a dye-doped SiO_2@MnO_2 core–shell nanocomposite, which is designed as a multifunctional nanoprobe for detecting GSH and recognizing cancer cells, provided a simple

sequencing technique was provided to develop an intelligent theragnostics platform.[80] In this method, the porous MnO_2 shell serves as the acceptor and the fluorescein isothiocyanate (FITC)-doped solid SiO_2 nanosphere (FS) serves as the donor. Methylene blue (MB), a photosensitizer, is immobilized into the porous MnO_2 pores for exploiting the therapeutic potential of the nanoplatform. The photosensitizer is then guaranteed to be internalized in tumour cells by the poly(ethylene glycol) (PEG) on the outer layer, which serves as a "gatekeeper." To perceive the sequence procedure, the high GSH levels in the cells would efficiently destroy the MnO_2 layer once the nanocomposite enters the tumour cell. This will generate more Mn^{2+}, release methylene blue for the purpose of therapeutic application as a photosensitizer, and restore the fluorescence of the FITC leading to the GSH detection. With a limit of detection of 2.1 μM, the linearity could be attained with GSH concentrations, which also satisfy the needs of actual human serum GSH detectives.

A strategy for the GSH detection was demonstrated by releasing glucose from MnO_2 nanosheet-gated mesoporous silica nanoparticles (MSNs) as a target induced release nanobiosensor.[24] Due to the high favourable interaction between glucose and silica walls, substantial quantities of glucose were first loaded into the pores of MSNs. The electrostatic interaction causes negatively charged MnO_2 nanosheets to then seal the gates of positively charged aminated MSNs. MSN-G@MnO_2
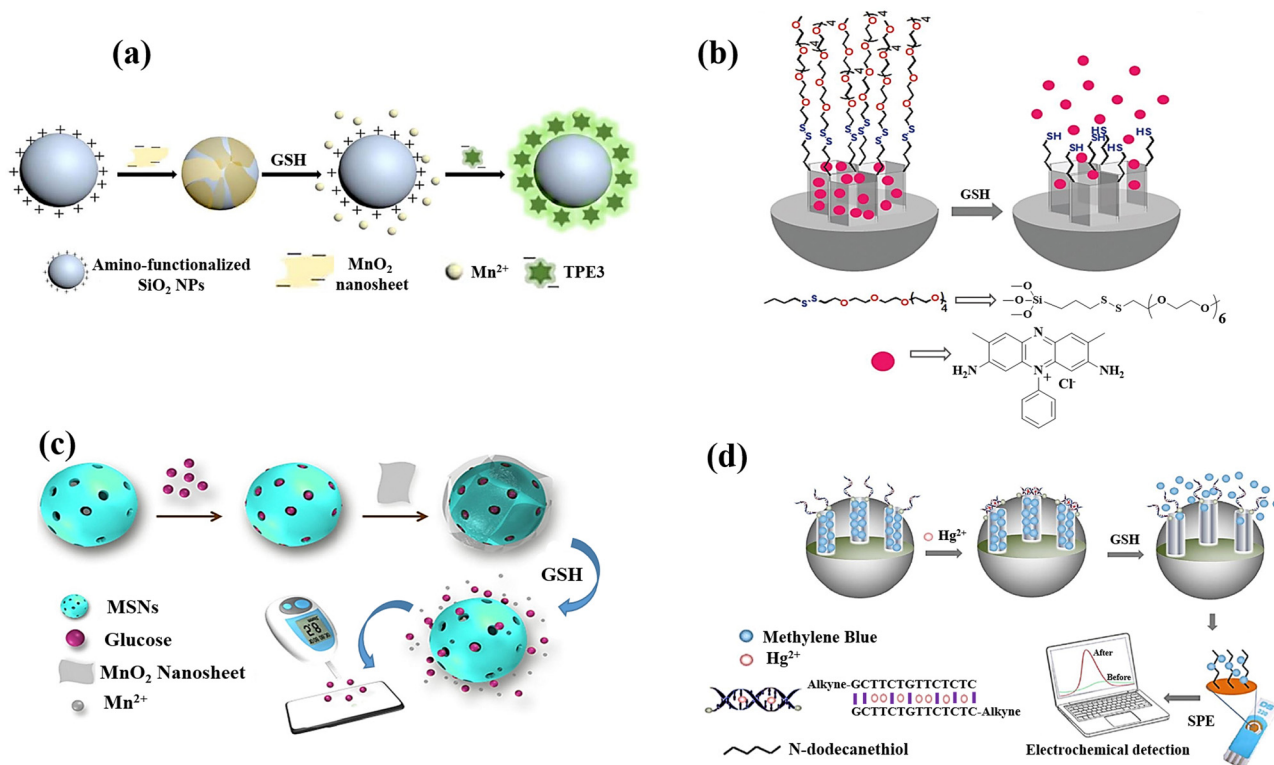

Fig. 12 (a) Schematic exhibiting the label-free fluorescence "turn-on" for detecting GSH by employing MnO_2 nanosheets assisted aggregation-induced emission-silica nanoparticles (AIE-SiO_2).[23] (b) Mesoporous silica nanoparticles containing safranin O and coated with oligo(ethylene glycol) chains containing disulfide were employed in the fluorimetry GSH detection.[79] (c) Preparation of the MnO_2-nanosheet-gated MSNs and the utilization of an external PGM for quantitative GSH detection.[24] (d) Diagram of synthesis of $Co_3(BTC)_2 \cdot 12H_2O$ and mixed-valence-state cobalt (MVSC), as well as colourimetric sensor for GSH detection[81] reproduced with the permission of Elsevier, Royal Society of Chemistry, and Springer Nature.

This journal is © The Royal Society of Chemistry 2024

J. Mater. Chem. B, 2024, 12, 8285–8309 | 8303

begins to decompose upon the addition of GSH due to the dissociation of MnO$_2$. Due to the "gate" being removed, the pore-trapped glucose could diffuse outside of MSNs for personal glucosemeter (PGM) detection, and the GSH concentration is correlated to the obtained PGM signal (Fig. 12(c)).

An electrochemical assay based on n-dodecanethiol modified screen-printed electrode (SPE) was created in order to quickly and directly detect GSH using MSNs and DNA biogate.[81] It was intended to create a covalently modified DNA molecule-gated switch in order to implement the mechanism of gating. For this purpose, the T-rich DNA regions on the MSN hybridized surface with one another by the T–Hg^{2+}–T base pair to construct a double-stranded configuration in the presence of Hg^{2+} ions, blocking pores and concentrating electroactive molecules, which was methylene blue (MB). When GSH is present, the T–Hg^{2+}–T complex experienced a competitive displacement reaction that might cause the transformation of duplex DNA into single-stranded DNA, opening- the pores. As a result, GSH molecules cause the entrapped electroactive molecules in MSN-dsDNA to be released. Furthermore, the n-dodecanethiol modified SPE can be used to quantify the electroactive molecules produced from MSN-dsDNA, and the formed differential pulse voltammetry (DPV) signal provides a definitive connection with the GSH levels.

The preparation of a nanoporous silicon chip loaded with AuNPs was reported for surface-assisted laser desorption/ionization mass spectrometry (SALDI-MS) analysis of GSH molecule.[165] Based on the chemical etching method using metal assistance, a flat silicon surface was etched into a nanoporous structure (100 nm cavity network) and the AgNPs were loaded in the bottom of the nanopores by Ag assisted

chemical etching process silicon surface followed by AuNPs coating on the ridges using the in situ synthesis of AuNPs on the nanocavity (Fig. 13). By using Au–S binding, AuNPs on nanostructured silicon precisely caught thiol compounds from complex samples. Since a 337 nm laser can destroy the Au–S binding, the thiol molecules adsorbed on the AuNPs were desorbed and ionized which is detected by SALDI-MS analysis.

8. Advantages and challenges in nanomaterial–based GSH Sensor development

Different types of nanomaterials mentioned in this review offer advantages for GSH sensing. For instance, carbon-based nanomaterials, such as carbon dots and graphene quantum dots, offer significant advantages for sensing applications due to their intrinsic fluorescence and electronic properties. Their strong, tuneable fluorescence provides high sensitivity and specificity in optical detection, while their excellent electrical conductivity enhances electron transfer processes in electrochemical sensing, resulting in improved response times and lower detection limits.[16,97] In addition, polymeric-based nanomaterials, such as conjugated polymers and polymer dots, offer significant advantages for GSH sensing due to their fluorescence properties and their functionalization capability. These materials can be easily functionalized with a variety of chemical groups, biomolecules, and nanoparticles.[17,105] On the other hand, MOFs, with their customizable metal–organic compositions, and COFs, with covalently bonded organic networks, can be designed to mimic enzymatic reactions effectively, offering
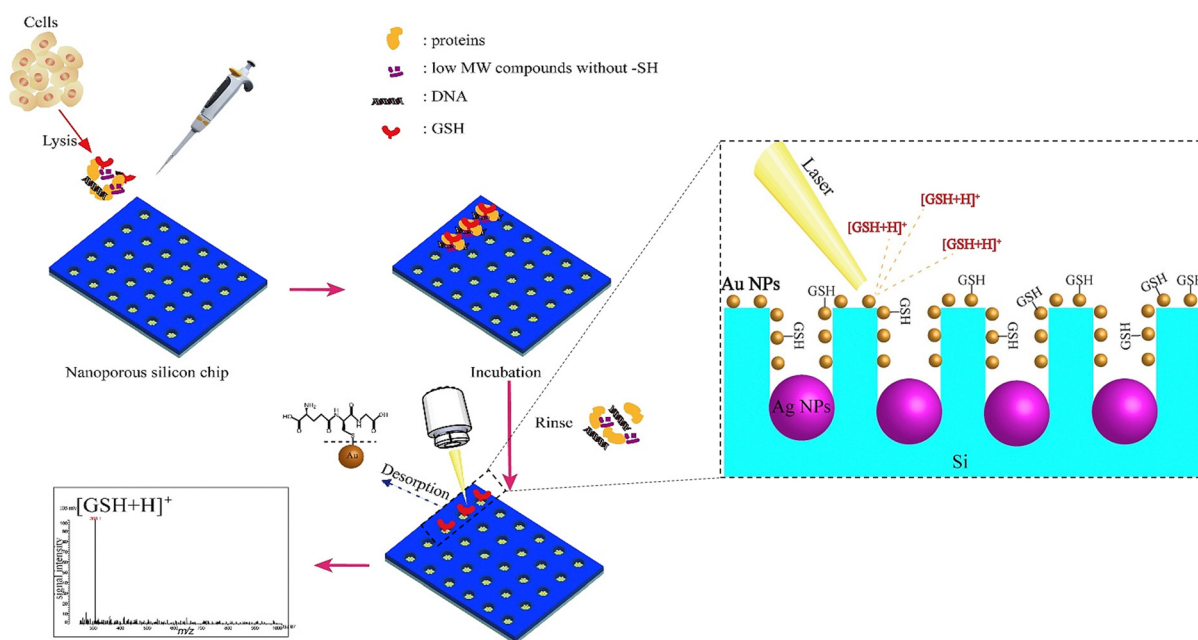

Fig. 13 Schematic illustrating the examination of cells. The nanostructured sample spots were loaded with 2 μL of cell lysate, and they were incubated for 10 minutes. The sample spot was cleaned with deionized water and dried in preparation for SALDI-MS analysis after the leftover lysate solution was removed. Reproduced from ref. 165 with the permission of Elsevier.

robust and sensitive platforms for sensing applications targeting GSH.[120] QDs are also ideal for GSH sensing due to their small size and tuneable fluorescence properties, which vary with size. This size-dependent fluorescence enables precise detection of GSH concentrations, making QDs valuable for developing sensitive biosensors in biomedical and environmental applications.[136] Gold nanomaterials present significant advantages in GSH sensing due to their tuneable surface plasmon resonance, catalytic activities, and distinct electrochemical behaviour. The tuneable surface plasmon resonance of gold nanoparticles allows for precise control over their optical properties, enhancing sensitivity in optical sensing methods. Additionally, their catalytic properties facilitate redox reactions relevant to GSH detection, while their unique electrochemical behaviour enables sensitive detection in electrochemical sensors.[144] On the other hand, silicon-based nanomaterials offer a distinct advantage in GSH sensing as substrates for loading dyes or nanoparticles due to their porous structures and large surface areas. These properties enable efficient loading and immobilization of dyes or nanoparticles, enhancing the sensitivity for GSH detection.[155]

While these nanomaterials have been explored for the detection of GSH, there are specific challenges associated with the development of nanomaterials for GSH sensing. Nanomaterials used for GSH sensing should exhibit stability over time, especially when exposed to biological environments.[166] Factors such as degradation, aggregation, or changes in surface properties can impact the long-term performance of the sensor. The selected nanomaterials should be biocompatible to avoid adverse effects on cellular function or viability. The interaction of nanomaterials with biological systems should be carefully considered to ensure minimal cytotoxicity.[167–169] Reproducibility is a critical factor for the practical implementation of GSH sensors.[170] Variations in the synthesis and functionalization of nanomaterials can impact the reproducibility of sensor responses, making it challenging to obtain consistent results. Continuous and real-time monitoring of GSH levels in living cells or tissues is desirable for understanding dynamic cellular processes.[171] Developing nanomaterial-based sensors capable of real-time monitoring without causing cellular perturbations is a technological challenge.[172] The irreversibility of the sensor response can be a challenge in the development of GSH sensors using nanomaterials.[173] To put it differently, most of nanomaterial-based sensors rely on chemical reactions with GSH for signal transduction. These reactions may result in the formation of irreversible products or alterations to the sensor's surface chemistry. The irreversible nature of these reactions can limit the sensor's ability to be reset for subsequent measurements. In addition, these nano-biosensors may undergo irreversible aggregation or morphological changes in the biological environments[174] leading to negative impact on the sensor's performance. Most importantly, irreversible nanomaterials used for intracellular GSH sensing may interfere with cellular processes and contribute to GSH depletion triggering cellular responses,[175] including GSH consumption as part of the cell's defence mechanism against perceived stress, which

results in alterations in GSH levels over time. Due to these limitations, the majority of nanomaterial-based GSH sensors cannot be applied as the real time intracellular GSH sensors and have been utilized predominantly for qualitative GSH detection in the biological environments and intracellular GSH assessments.

9. Future prospects

The enhancement of nanomaterials application for GSH sensing involves a combination of innovative strategies and approaches in sensor design, fabrication, and application. For instance, investigating and designing of nanomaterials with high selectivity for GSH by incorporating specific recognition elements, such as aptamers or molecularly imprinted polymers, as well as molecular engineering and advanced surface modifications can enhance the specificity of sensors. In other words, printing technologies, such as inkjet or screen printing, allow for the precise deposition of functional materials onto sensor surfaces enabling the selective functionalization of nanomaterials with recognition elements specific to GSH, such as aptamers, antibodies, or molecularly imprinted polymers, and the controlled placement of these elements enhances the sensor's selectivity for GSH. Regarding the compatibility and solubility in the biological environment, by introducing hydrophilic or amphiphilic functional groups to develop multifunctional nanomaterials, they can become more dispersible in aqueous solutions, enhancing their compatibility with biological environments and facilitate better cellular uptake, ensuring efficient interaction with intracellular environments for GSH detection within living cells. For the long-term stability enhancement, incorporation of protective coatings or encapsulation strategies to improve the long-term stability of nanomaterial-based GSH sensors can prevent degradation and maintain sensor performance over extended periods, especially in biological environments.

Addressing the challenges related to the irreversibility of nanomaterials in the context of GSH sensing requires meticulous consideration of strategic design principles and the implementation of methodological approaches. For example, design of nanomaterials that undergo reversible interactions with GSH, which involves selecting materials or surface modifications that allow for the regeneration of the sensor after GSH detection, enables repeated and reliable measurements. Moreover, implementing dynamic coatings on nanomaterial surfaces that can be controlled or triggered to revert to their original state, such as the use of stimuli-responsive polymers or coatings that respond to specific conditions, results in reversibility in GSH sensing for nanomaterial-based GSH sensors and flexibility of these sensors since they become adaptable to variations of GSH levels in the intracellular environment.

10. Conclusions

In summary, nanostructured materials have become pivotal in developing highly sensitive chemo-sensors and biosensors over

This journal is © The Royal Society of Chemistry 2024

J. Mater. Chem. B, 2024, **12**, 8285–8309 | **8305**

the past two decades, primarily due to their exceptional properties. This review has specifically focused on exploring recent advancements in the fabrication of nanomaterials for detecting GSH a crucial biomolecule implicated in various physiological and pathological processes. By utilizing different categories of materials, including carbon, polymeric, metal–organic frameworks (MOFs), covalent organic frameworks (COFs), quantum dots (QDs), and metal-based and silicon-based nanomaterials, researchers have been able to create chemo- and biosensors with improved sensitivity and selectivity for GSH detection. Despite their promise, challenges persist in maintaining stability in biological environments, ensuring biocompatibility, and addressing irreversibility issues. Future advancements may involve incorporating specific recognition elements, enhancing compatibility in biological environments, and implementing protective coatings or encapsulation strategies for long-term stability. Overall, nanomaterial-based sensors offer significant potential for enhancing our understanding of GSH dynamics and developing innovative diagnostic and therapeutic approaches for various diseases. Addressing current challenges and implementing innovative design strategies will be crucial in realizing this potential.

Author contributions

Saman Bagherpour was responsible for the conceptualization, investigation, visualization, and writing – original draft, review & editing. Lluïsa Pérez-García was responsible for conceptualization, investigation, visualization, supervision, funding acquisition, and writing – original draft, review & editing.

Data availability

No primary research results, software or code have been included and no new data were generated or analysed as part of this review.

Conflicts of interest

The authors declare no conflict of interest.

Acknowledgements

References

1 A. K. Bachhawat and S. Yadav, *IUBMB Life*, 2018, **70**, 585–592.

2 Y.-T. Chiang, Y.-W. Yen and C.-L. Lo, *Biomaterials*, 2015, **61**, 150–161.

3 N. Couto, J. Wood and J. Barber, *Free Radical Biol. Med.*, 2016, **95**, 27–42.

4 N. F. Atta, A. Galal and S. M. Azab, *Anal. Bioanal. Chem.*, 2012, **404**, 1661–1672.

5 J. M. May, Z. Qu and X. Li, *Biochem. Pharmacol.*, 2001, **62**, 873–881.

6 M. Hanko, Ľ. Švorc, A. Planková and P. Mikuš, *Anal. Chim. Acta*, 2019, **1062**, 1–27.

7 M. Smeyne and R. J. Smeyne, *Free Radical Biol. Med.*, 2013, **62**, 13–25.

8 P. K. Mandal, S. Saharan, M. Tripathi and G. Murari, *Biol. Psychiatry*, 2015, **78**, 702–710.

9 M. Sharma, S. Gupta, K. Singh, M. Mehndiratta, A. Gautam, O. P. Kalra, R. Shukla and J. K. Gambhir, *Diabetes Metab. Syndr.*, 2016, **10**, 194–197.

10 Y. Zhu, P. M. Carvey and Z. Ling, *Brain Res.*, 2006, **1090**, 35–44.

11 S. Weschawalit, S. Thongthip, P. Phutrakool and P. Asawanonda, *Clin., Cosmet. Invest. Dermatol.*, 2017, **10**, 147–153.

12 E. C. Lien, C. A. Lyssiotis, A. Juvekar, H. Hu, J. M. Asara, L. C. Cantley and A. Toker, *Nat. Cell Biol.*, 2016, **18**, 572–578.

13 M. P. Gamcsik, M. S. Kasibhatla, S. D. Teeter and O. M. Colvin, *Biomarkers*, 2012, **17**, 671–691.

14 L. Kennedy, J. K. Sandhu, M.-E. Harper and M. Cuperlovic-Culf, *Biomolecules*, 2020, 10.

15 H. Wang, H. Jiang, C. Corbet, S. de Mey, K. Law, T. Gevaert, O. Feron and M. De Ridder, *Cancer Lett.*, 2019, **450**, 42–52.

16 A. Dalla Colletta, M. Pelin, S. Sosa, L. Fusco, M. Prato and A. Tubaro, *Carbon*, 2022, **196**, 683–698.

17 A. P. Singh, A. Biswas, A. Shukla and P. Maiti, *Signal Transduction Targeted Ther.*, 2019, **4**, 33.

18 T. Han, J. Yang, Y. Wang, Y. Cao, Y. Wang, H.-Y. Chen and J.-J. Zhu, *Electrochim. Acta*, 2021, **381**, 138281.

19 J. Xie, D. Cheng, P. Li, Z. Xu, X. Zhu, Y. Zhang, H. Li, X. Liu, M. Liu and S. Yao, *ACS Appl. Nano Mater.*, 2021, **4**, 4853–4862.

20 Y. Peng, M. Huang, L. Chen, C. Gong, N. Li, Y. Huang and C. Cheng, *Nano Res.*, 2022, **15**, 8783–8790.

21 Q. Zhai, H. Xing, D. Fan, X. Zhang, J. Li and E. Wang, *Sens. Actuators, B*, 2018, **273**, 1827–1832.

22 B. Chen and F. Wang, *Nanoscale*, 2018, **10**, 19898–19905.

23 X. Zhang, R. Kong, Q. Tan, F. Qu and F. Qu, *Talanta*, 2017, **169**, 1–7.

24 Q. Tan, R. Zhang, R. Kong, W. Kong, W. Zhao and F. Qu, *Microchim. Acta*, 2017, **185**, 44.

25 D. Chen and Y. Feng, *Crit. Rev. Anal. Chem.*, 2022, **52**, 649–666.

26 J. Zhang, N. Wang, X. Ji, Y. Tao, J. Wang and W. Zhao, *Chem. – Eur. J.*, 2020, **26**, 4172–4192.

27 X. Sun, F. Guo, Q. Ye, J. Zhou, J. Han and R. Guo, *Biosensors*, 2023, 13.

28 C.-X. Yin, K.-M. Xiong, F.-J. Huo, J. C. Salamanca and R. M. Strongin, *Angew. Chem., Int. Ed.*, 2017, **56**, 13188–13198.

8306 | *J. Mater. Chem. B*, 2024, **12**, 8285–8309

This journal is © The Royal Society of Chemistry 2024

29 S. Wang, Y. Huang and X. Guan, *Molecules*, 2021, 26.

30 J. Dai, C. Ma, P. Zhang, Y. Fu and B. Shen, *Dyes Pigm.*, 2020, **177**, 108321.

31 T. A. Fayed, M. N. El-Nahass, H. A. El-Daly and A. A. Shokry, *Appl. Organomet. Chem.*, 2019, **33**, e4868.

32 R. Gui, H. Guo and H. Jin, *Nanoscale Adv.*, 2019, **1**, 3325–3363.

33 J. Lei and H. Ju, *Chem. Soc. Rev.*, 2012, **41**, 2122–2134.

34 L. Lan, Y. Yao, J. Ping and Y. Ying, *Biosens. Bioelectron.*, 2017, **91**, 504–514.

35 V. Biju, *Chem. Soc. Rev.*, 2014, **43**, 744–764.

36 G. Konvalina and H. Haick, *Acc. Chem. Res.*, 2014, **47**, 66–76.

37 O. N. J. Oliveira, R. M. Iost, J. R. J. Siqueira, F. N. Crespilho and L. Caseli, *ACS Appl. Mater. Interfaces*, 2014, **6**, 14745–14766.

38 C. F. Markwalter, A. G. Kantor, C. P. Moore, K. A. Richardson and D. W. Wright, *Chem. Rev.*, 2019, **119**, 1456–1518.

39 D. de Melo-Diogo, C. Pais-Silva, D. R. Dias, A. F. Moreira and I. J. Correia, *Adv. Healthcare Mater.*, 2017, **6**, 1700073.

40 K. P. Loh, D. Ho, G. N. C. Chiu, D. T. Leong, G. Pastorin and E. K.-H. Chow, *Adv. Mater.*, 2018, **30**, 1802368.

41 Y. Lu, W. Sun and Z. Gu, *J. Controlled Release*, 2014, **194**, 1–19.

42 C. Yang, X. Wang, H. Liu, S. Ge, M. Yan, J. Yu and X. Song, *Sens. Actuators, B*, 2017, **248**, 639–645.

43 Z. Li, J. Zhang, Y. Li, S. Zhao, P. Zhang, Y. Zhang, J. Bi, G. Liu and Z. Yue, *Biosens. Bioelectron.*, 2018, **99**, 251–258.

44 H. Zhang, J. Chen, Y. Yang, L. Wang, Z. Li and H. Qiu, *Anal. Chem.*, 2019, **91**, 5004–5010.

45 S. Rostami, A. Mehdinia, R. Niroumand and A. Jabbari, *Anal. Chim. Acta*, 2020, **1120**, 11–23.

46 P. Lei, Y. Zhou, R. Zhu, Y. Liu, C. Dong and S. Shuang, *Sens. Actuators, B*, 2019, **297**, 126756.

47 Z. Song, F. Quan, Y. Xu, M. Liu, L. Cui and J. Liu, *Carbon*, 2016, **104**, 169–178.

48 D. Wu, G. Li, X. Chen, N. Qiu, X. Shi, G. Chen, Z. Sun, J. You and Y. Wu, *Microchim. Acta*, 2017, **184**, 1923–1931.

49 C. Yang, X. Wang, H. Liu, S. Ge, J. Yu and M. Yan, *New J. Chem.*, 2017, **41**, 3374–3379.

50 A. K. Saini and S. K. Sahoo, *J. Photochem. Photobiol., A*, 2022, **430**, 113987.

51 L. Han, S. G. Liu, X. F. Zhang, B. X. Tao, N. B. Li and H. Q. Luo, *Sens. Actuators, B*, 2018, **258**, 25–31.

52 J. Zhang, W. Pei, Q. Xu, H. Jiang and J. Chen, *Sens. Actuators, B*, 2022, **357**, 131417.

53 C. Li, X. Zhang, Y. Guo, F. Seidi, X. Shi and H. Xiao, *ACS Appl. Mater. Interfaces*, 2021, **13**, 19756–19767.

54 Q. Li, A. Sun, Y. Si, M. Chen and L. Wu, *Chem. Mater.*, 2017, **29**, 6758–6765.

55 J.-S. Luo, Y.-P. Jin, Y.-M. Guo and Q. Li, *Inorg. Chem. Commun.*, 2022, **138**, 109307.

56 T. Zhang, H. Li, M. Liu, H. Zhou, Z. Zhang, C. Yu, C. Wang and G. Wang, *Sens. Actuators, B*, 2021, **341**, 129987.

57 J. Sun, N. Chen, X. Chen, Q. Zhang and F. Gao, *Anal. Chem.*, 2019, **91**, 12414–12421.

58 C. Gong, Z. Li, G. Liu, R. Wang and S. Pu, *Spectrochim. Acta, Part A*, 2022, **265**, 120362.

59 H. Yang, J. Liu, L. Wang, L. Ma, F. Nie and G. Yang, *Talanta*, 2022, **238**, 123041.

60 G. Li, W. Ma, Y. Yang, C. Zhong, H. Huang, D. Ouyang, Y. He, W. Tian, J. Lin and Z. Lin, *ACS Appl. Mater. Interfaces*, 2021, **13**, 49482–49489.

61 P. Jin, X. Niu, F. Zhang, K. Dong, H. Dai, H. Zhang, W. Wang, H. Chen and X. Chen, *ACS Appl. Mater. Interfaces*, 2020, **12**, 20414–20422.

62 F. Qu, H. Yan, K. Li, J. You and W. Han, *J. Mater. Sci.*, 2020, **55**, 10022–10034.

63 N. He, X. Zhu, F. Liu, R. Yu, Z. Xue and X. Liu, *Chem. Eng. J.*, 2022, **445**, 136543.

64 W. Zeng, L. Liu, Y. Yi, Y. Wu, N. Sun, B. Lv and G. Zhu, *Microchem. J.*, 2019, **150**, 104149.

65 W. Luo, H. Liu, X. Liu, L. Liu and W. Zhao, *Colloids Surf., B*, 2021, **201**, 111631.

66 P. Jia, J. Hou, K. Yang and L. Wang, *Microchim. Acta*, 2021, **188**, 299.

67 J. Zeng, X.-W. Hua, Y.-W. Bao and F.-G. Wu, *ACS Appl. Nano Mater.*, 2021, **4**, 6083–6092.

68 F. Yan, Z. Sun, J. Xu, H. Li and Y. Zhang, *Microchim. Acta*, 2020, **187**, 344.

69 B. Zhang, P. Zou, J. Li, D. Lu, X. Wang and L. Ma, *ACS Appl. Nano Mater.*, 2022, **5**, 4677–4687.

70 H. Li, R. Xie, C. Huang, J. He, P. Yang, J. Tao, B. Lin and P. Zhao, *Sens. Actuators, B*, 2020, **321**, 128518.

71 J.-F. Li, P.-C. Huang and F.-Y. Wu, *Sens. Actuators, B*, 2017, **240**, 553–559.

72 H.-H. Pang, Y.-C. Ke, N.-S. Li, Y.-T. Chen, C.-Y. Huang, K.-C. Wei and H.-W. Yang, *Biosens. Bioelectron.*, 2020, **165**, 112325.

73 J. Feng, P. Huang, S. Shi, K.-Y. Deng and F.-Y. Wu, *Anal. Chim. Acta*, 2017, **967**, 64–69.

74 S. Chu, H. Wang, Y. Du, F. Yang, L. Yang and C. Jiang, *ACS Sustainable Chem. Eng.*, 2020, **8**, 8175–8183.

75 P. Singh, R. P. Ojha, S. Kumar, A. K. Singh and R. Prakash, *Mater. Chem. Phys.*, 2021, **267**, 124684.

76 H. Li, Y. Wen, X. Zhu, J. Wang, L. Zhang and B. Sun, *ACS Sustainable Chem. Eng.*, 2020, **8**, 520–526.

77 T. Wang, P. Su, F. Lin, Y. Yang and Y. Yang, *Sens. Actuators, B*, 2018, **254**, 329–336.

78 R. Kaimal, V. Vinoth, A. Shrikrishna Salunke, H. Valdés, R. Viswanathan Mangalaraja, B. Aljafari and S. Anandan, *Ultrason. Sonochem.*, 2022, **82**, 105868.

79 S. El Sayed, C. Giménez, E. Aznar, R. Martínez-Máñez, F. Sancenón and M. Licchelli, *Org. Biomol. Chem.*, 2015, **13**, 1017–1021.

80 Y. Zhang, D. Wang, Y. Meng, W. Lu, S. Shuang and C. Dong, *ACS Sustainable Chem. Eng.*, 2021, **9**, 2770–2783.

81 Y. Wang, L. Jiang, L. Chu, W. Liu, S. Wu, Y. Wu, X. He and K. Wang, *Biosens. Bioelectron.*, 2017, **87**, 459–465.

This journal is © The Royal Society of Chemistry 2024

J. Mater. Chem. B, 2024, **12**, 8285–8309 | **8307**

82 D. Maiti, X. Tong, X. Mou and K. Yang, *Front. Pharmacol.*, 2019, **9**, 1401.

83 J. R. Siqueira and O. N. Oliveira, *Carbon-Based Nanomaterials. Nanostructures*, ed. A. L Da Róz, M. Ferreira, F. de Lima Leite and O. N. B. T.-N. Oliveira, William Andrew Publishing, 2017, ch. 9, pp. 233–249.

84 P. W. Dunk, N. K. Kaiser, C. L. Hendrickson, J. P. Quinn, C. P. Ewels, Y. Nakanishi, Y. Sasaki, H. Shinohara, A. G. Marshall and H. W. Kroto, *Nat. Commun.*, 2012, **3**, 855.

85 N. Gupta, S. M. Gupta and S. K. Sharma, *Carbon Lett.*, 2019, **29**, 419–447.

86 C. Chung, Y.-K. Kim, D. Shin, S.-R. Ryoo, B. H. Hong and D.-H. Min, *Acc. Chem. Res.*, 2013, **46**, 2211–2224.

87 M. Chipaux, K. J. van der Laan, S. R. Hemelaar, M. Hasani, T. Zheng and R. Schirhagl, *Small*, 2018, **14**, 1704263.

88 M. F. Naief, S. N. Mohammed, H. J. Mayouf and A. M. Mohammed, *J. Organomet. Chem.*, 2023, **999**, 122819.

89 J. Lin, Y. Huang and P. Huang, in *Micro and Nano Technologies*, ed. B. Sarmento and J. das Neves, Elsevier, 2018, pp. 247–287.

90 J. Bartelmess, S. J. Quinn and S. Giordani, *Chem. Soc. Rev.*, 2015, **44**, 4672–4698.

91 S. H. Ku, M. Lee and C. B. Park, *Adv. Healthcare Mater.*, 2013, **2**, 244–260.

92 Z. Peng, T. Zhao, Y. Zhou, S. Li, J. Li and R. M. Leblanc, *Adv. Healthcare Mater.*, 2020, **9**, 1901495.

93 Z. Wang and Z. Dai, *Nanoscale*, 2015, **7**, 6420–6431.

94 R. Eivazzadeh-Keihan, E. Bahojb Noruzi, E. Chidar, M. Jafari, F. Davoodi, A. Kashtiaray, M. Ghafori Gorab, S. Masoud Hashemi, S. Javanshir, R. Ahangari Cohan, A. Maleki and M. Mahdavi, *Chem. Eng. J.*, 2022, **442**, 136183.

95 H. Zare, S. Ahmadi, A. Ghasemi, M. Ghanbari, N. Rabiee, M. Bagherzadeh, M. Karimi, T. J. Webster, M. R. Hamblin and E. Mostafavi, *Int. J. Nanomed.*, 2021, **16**, 1681–1706.

96 S. Taghavi, K. Abnous, S. M. Taghdisi, M. Ramezani and M. Alibolandi, *J. Controlled Release*, 2020, **318**, 158–175.

97 K. D. Patel, R. K. Singh and H.-W. Kim, *Mater. Horiz.*, 2019, **6**, 434–469.

98 Z. Li, L. Wang, Y. Li, Y. Feng and W. Feng, *Compos. Sci. Technol.*, 2019, **179**, 10–40.

99 S. Chen, Y.-L. Yu and J.-H. Wang, *Anal. Chim. Acta*, 2018, **999**, 13–26.

100 H. Tan, Q. Li, Z. Zhou, C. Ma, Y. Song, F. Xu and L. Wang, *Anal. Chim. Acta*, 2015, **856**, 90–95.

101 P. W. Riddles, R. L. Blakeley and B. Zerner, *Anal. Biochem.*, 1979, **94**, 75–81.

102 F. Canfarotta, M. J. Whitcombe and S. A. Piletsky, *Biotechnol. Adv.*, 2013, **31**, 1585–1599.

103 M. Elsabahy, G. S. Heo, S.-M. Lim, G. Sun and K. L. Wooley, *Chem. Rev.*, 2015, **115**, 10967–11011.

104 O. R. Miranda, X. Li, L. Garcia-Gonzalez, Z.-J. Zhu, B. Yan, U. H. F. Bunz and V. M. Rotello, *J. Am. Chem. Soc.*, 2011, **133**, 9650–9653.

105 S. Kango, S. Kalia, A. Celli, J. Njuguna, Y. Habibi and R. Kumar, *Prog. Polym. Sci.*, 2013, **38**, 1232–1261.

106 W.-K. Oh, O. S. Kwon and J. Jang, *Polym. Rev.*, 2013, **53**, 407–442.

107 X. Ji, W. Wang, X. Li, Y. Chen and C. Ding, *Talanta*, 2016, **150**, 666–670.

108 C. Zhang, L. Gong, L. Xiang, Y. Du, W. Hu, H. Zeng and Z.-K. Xu, *ACS Appl. Mater. Interfaces*, 2017, **9**, 30943–30950.

109 F. Gao, J. Sun and Q. Zhang, in *Woodhead Publishing Series in Electronic and Optical Materials*, ed. K. Y. Cheong, M. A. Fraga, P. Sonar, R. S. Pessoa and J. Casanova-Moreno, Woodhead Publishing, 2024, pp. 27–52.

110 M. Verma, Y.-H. Chan, S. Saha and M.-H. Liu, *ACS Appl. Bio Mater.*, 2021, **4**, 2142–2159.

111 Z. Ding, X. Dou, G. Wu, C. Wang and J. Xie, *Talanta*, 2023, **259**, 124494.

112 M. Ding, R. W. Flaig, H.-L. Jiang and O. M. Yaghi, *Chem. Soc. Rev.*, 2019, **48**, 2783–2828.

113 I. Nath, J. Chakraborty and F. Verpoort, *Chem. Soc. Rev.*, 2016, **45**, 4127–4170.

114 D. Wang, D. Jana and Y. Zhao, *Acc. Chem. Res.*, 2020, **53**, 1389–1400.

115 L. Jiao, Y. Wang, H.-L. Jiang and Q. Xu, *Adv. Mater.*, 2018, **30**, 1703663.

116 X. Niu, X. Li, Z. Lyu, J. Pan, S. Ding, X. Ruan, W. Zhu, D. Du and Y. Lin, *Chem. Commun.*, 2020, **56**, 11338–11353.

117 X. Zhong, H. Xia, W. Huang, Z. Li and Y. Jiang, *Chem. Eng. J.*, 2020, **381**, 122758.

118 H. Furukawa, K. E. Cordova, M. O'Keeffe and O. M. Yaghi, *Science*, 2013, **341**, 1230444.

119 Y. He, W. Zhou, G. Qian and B. Chen, *Chem. Soc. Rev.*, 2014, **43**, 5657–5678.

120 L. Zhu, X.-Q. Liu, H.-L. Jiang and L.-B. Sun, *Chem. Rev.*, 2017, **117**, 8129–8176.

121 P. Kumar, A. Deep and K.-H. Kim, *TrAC, Trends Anal. Chem.*, 2015, **73**, 39–53.

122 W. P. Lustig, S. Mukherjee, N. D. Rudd, A. V. Desai, J. Li and S. K. Ghosh, *Chem. Soc. Rev.*, 2017, **46**, 3242–3285.

123 H. D. Lawson, S. P. Walton and C. Chan, *ACS Appl. Mater. Interfaces*, 2021, **13**, 7004–7020.

124 T. Liu, M. Zhou, Y. Pu, L. Liu, F. Li, M. Li and M. Zhang, *Sens. Actuators, B*, 2021, **342**, 130047.

125 N. V. de Almeida Ferraz, W. Silva Vasconcelos, C. Santos Silva, S. Alves Junior, C. G. Amorim, M. da Conceição Branco, S. M. Montenegro and M. C. da Cunha Areias, *Sens. Actuators, B*, 2020, **307**, 127636.

126 C. S. Diercks and O. M. Yaghi, *Science*, 2017, **355**, eaal1585.

127 J. Guo and D. Jiang, *ACS Cent. Sci.*, 2020, **6**, 869–879.

128 M. Li, S. Qiao, Y. Zheng, Y. H. Andaloussi, X. Li, Z. Zhang, A. Li, P. Cheng, S. Ma and Y. Chen, *J. Am. Chem. Soc.*, 2020, **142**, 6675–6681.

129 P. She, Y. Qin, X. Wang and Q. Zhang, *Adv. Mater.*, 2022, **34**, 2101175.

130 P. J. Waller, F. Gándara and O. M. Yaghi, *Acc. Chem. Res.*, 2015, **48**, 3053–3063.

8308 | *J. Mater. Chem. B*, 2024, **12**, 8285–8309

This journal is © The Royal Society of Chemistry 2024

131 M. Zhao, H.-B. Wang, L.-N. Ji and Z.-W. Mao, *Chem. Soc. Rev.*, 2013, **42**, 8360–8375.

132 L. Zhang, Z. Liu, Q. Deng, Y. Sang, K. Dong, J. Ren and X. Qu, *Angew. Chem., Int. Ed.*, 2021, **60**, 3469–3474.

133 O. E. Semonin, J. M. Luther and M. C. Beard, *Mater. Today*, 2012, **15**, 508–515.

134 T. Frecker, D. Bailey, X. Arzeta-Ferrer, J. McBride and S. J. Rosenthal, *ECS J. Solid State Sci. Technol.*, 2016, **5**, R3019.

135 S. Kargozar, S. J. Hoseini, P. B. Milan, S. Hooshmand, H.-W. Kim and M. Mozafari, *Biotechnol. J.*, 2020, **15**, 2000117.

136 T. Jamieson, R. Bakhshi, D. Petrova, R. Pocock, M. Imani and A. M. Seifalian, *Biomaterials*, 2007, **28**, 4717–4732.

137 A. Foerster and N. A. Besley, *J. Phys. Chem. A*, 2022, **126**, 2899–2908.

138 F. Zhang, Z. Ali, F. Amin, A. Riedinger and W. J. Parak, *Anal. Bioanal. Chem.*, 2010, **397**, 935–942.

139 K. D. Wegner and N. Hildebrandt, *Chem. Soc. Rev.*, 2015, **44**, 4792–4834.

140 Y. Zhou, L. Tang, G. Zeng, C. Zhang, X. Xie, Y. Liu, J. Wang, J. Tang, Y. Zhang and Y. Deng, *Talanta*, 2016, **146**, 641–647.

141 Y. Zhou, L. Tang, G. Zeng, C. Zhang, Y. Zhang and X. Xie, *Sens. Actuators, B*, 2016, **223**, 280–294.

142 N. Elahi, M. Kamali and M. H. Baghersad, *Talanta*, 2018, **184**, 537–556.

143 V. Amendola, R. Pilot, M. Frasconi, O. M. Maragò and M. A. Iatì, *J. Phys.: Condens. Matter*, 2017, **29**, 203002.

144 L. Qin, G. Zeng, C. Lai, D. Huang, P. Xu, C. Zhang, M. Cheng, X. Liu, S. Liu, B. Li and H. Yi, *Coord. Chem. Rev.*, 2018, **359**, 1–31.

145 X. Shi, W. Gu, B. Li, N. Chen, K. Zhao and Y. Xian, *Microchim. Acta*, 2014, **181**, 1–22.

146 M. Hasanzadeh, N. Shadjou and M. de la Guardia, *TrAC, Trends Anal. Chem.*, 2015, **72**, 1–9.

147 J. M. George, A. Antony and B. Mathew, *Microchim. Acta*, 2018, **185**, 358.

148 Y. Jia, X. Yi, Z. Li, L. Zhang, B. Yu, J. Zhang, X. Wang and X. Jia, *Talanta*, 2020, **219**, 121308.

149 B. Liu and J. Liu, *TrAC, Trends Anal. Chem.*, 2019, **121**, 115690.

150 O. Salim, K. A. Mahmoud, K. K. Pant and R. K. Joshi, *Mater. Today Chem.*, 2019, **14**, 100191.

151 M. Khazaei, A. Mishra, N. S. Venkataramanan, A. K. Singh and S. Yunoki, *Curr. Opin. Solid State Mater. Sci.*, 2019, **23**, 164–178.

152 Y. Chen, H. Chen and J. Shi, *Adv. Mater.*, 2013, **25**, 3144–3176.

153 R. Eivazzadeh-Keihan, K. K. Chenab, R. Taheri-Ledari, J. Mosafer, S. M. Hashemi, A. Mokhtarzadeh, A. Maleki and M. R. Hamblin, *Mater. Sci. Eng., C*, 2020, **107**, 110267.

154 C. Caltagirone, A. Bettoschi, A. Garau and R. Montis, *Chem. Soc. Rev.*, 2015, **44**, 4645–4671.

155 S. Jafari, H. Derakhshankhah, L. Alaei, A. Fattahi, B. S. Varnamkhasti and A. A. Saboury, *Biomed. Pharmacother.*, 2019, **109**, 1100–1111.

156 F. A. Harraz, *Sens. Actuators, B*, 2014, **202**, 897–912.

157 R. Moretta, L. De Stefano, M. Terracciano and I. Rea, *Sensors*, 2021, 21.

158 C. RoyChaudhuri, *Sens. Actuators, B*, 2015, **210**, 310–323.

159 K. Abnous, N. M. Danesh, M. Ramezani, S. M. Taghdisi and A. S. Emrani, *Anal. Methods*, 2018, **10**, 3232–3236.

160 A. Leidner, J. Bauer, M. Ebrahimi Khonachah, M. Takamiya, U. Strähle, T. Dickmeis, K. S. Rabe and C. M. Niemeyer, *Biomaterials*, 2019, **190–191**, 76–85.

161 S. Yang, M. Liu, F. Deng, L. Mao, Y. Yuan, H. Huang, J. Chen, L. Liu, X. Zhang and Y. Wei, *Appl. Surf. Sci.*, 2020, **510**, 145421.

162 S. Y. Tan, C. Teh, C. Y. Ang, M. Li, P. Li, V. Korzh and Y. Zhao, *Nanoscale*, 2017, **9**, 2253–2261.

163 L. Wang, B. Li, L. Zhang, L. Zhang and H. Zhao, *Sens. Actuators, B*, 2012, **171–172**, 946–953.

164 M. Becuwe, F. Cazier, P. Woisel and F. Delattre, *Colloids Surf., A*, 2013, **433**, 88–94.

165 J. Wang, M. Jie, H. Li, L. Lin, Z. He, S. Wang and J.-M. Lin, *Talanta*, 2017, **168**, 222–229.

166 R. Martínez, M. F. Navarro Poupard, A. Álvarez, E. Soprano, M. Migliavacca, C. Carrillo-Carrión, E. Polo, B. Pelaz and P. del Pino, in *Micro and Nano Technologies*, ed. E. J. Chung, L. Leon and C. Rinaldi, Elsevier, 2020, pp. 5–18.

167 M. Nikzamir, A. Akbarzadeh and Y. Panahi, *J. Drug Delivery Sci. Technol.*, 2021, **61**, 102316.

168 P. Xiong, X. Huang, N. Ye, Q. Lu, G. Zhang, S. Peng, H. Wang and Y. Liu, *Adv. Sci.*, 2022, **9**, 2106049.

169 A. Sani, C. Cao and D. Cui, *Biochem. Biophys. Rep.*, 2021, **26**, 100991.

170 L.-C. Chen, E. Wang, C.-S. Tai, Y.-C. Chiu, C.-W. Li, Y.-R. Lin, T.-H. Lee, C.-W. Huang, J.-C. Chen and W. L. Chen, *Biosens. Bioelectron.*, 2020, **155**, 112111.

171 M. L. Rogers and M. G. Boutelle, *Annu. Rev. Anal. Chem.*, 2013, **6**, 427–453.

172 Y.-L. Wu, N. Putcha, K. W. Ng, D. T. Leong, C. T. Lim, S. C. J. Loo and X. Chen, *Acc. Chem. Res.*, 2013, **46**, 782–791.

173 G. Rong, S. R. Corrie and H. A. Clark, *ACS Sens.*, 2017, **2**, 327–338.

174 C. D. Walkey and W. C. W. Chan, *Chem. Soc. Rev.*, 2012, **41**, 2780–2799.

175 C. Mytilineou, B. C. Kramer and J. A. Yabut, *Parkinsonism Relat. Disord.*, 2002, **8**, 385–387.

This journal is © The Royal Society of Chemistry 2024

J. Mater. Chem. B, 2024, **12**, 8285–8309 | 8309